

## Case History

# Exploring the model space and ranking a best class of models in surface-wave dispersion inversion: Application at European strong-motion sites

Giuseppe Di Giulio<sup>1</sup>, Alexandros Savvaidis<sup>2</sup>, Matthias Ohrnberger<sup>3</sup>, Marc Wathelet<sup>4</sup>, Cecile Cornou<sup>4</sup>, Brigitte Knapmeyer-Endrun<sup>3</sup>, Florence Renalier<sup>4</sup>, Nikos Theodoulidis<sup>2</sup>, and Pierre-Yves Bard<sup>4</sup>

### ABSTRACT

The inversion of surface-wave dispersion curve to derive shear-wave velocity profile is a very delicate process dealing with a nonunique problem, which is strongly dependent on the model space parameterization. When independent and reliable information is not available, the selection of most representative models within the ensemble produced by the inversion is often difficult. We implemented a strategy in the inversion of dispersion curves able to investigate the influence of the parameterization of the model space and to select a “best” class of models. We analyzed surface-wave dispersion curves measured at 14 European strong-motion sites within the NERIES EC-Project. We focused on the inversion task exploring the model space by means of four distinct parameterization classes composed of layers progressively added over a half-space. The classes differ in the definition of the shear-wave velocity profile; we considered models with uniform velocity as well as models

with increasing velocity with depth. At each site and for each model parameterization, we performed an extensive surface-wave inversion (200,100 models for five seeds) using the conditional neighborhood algorithm. We addressed the model evaluation following the corrected Akaike’s information criterion (AICc) that combines the concept of misfit to the number of degrees of freedom of the system. The misfit was computed as least-squares estimation between theoretical and observed dispersion curve. The model complexity was accounted in a penalty term by AICc. By applying such inversion strategy on 14 strong-motion sites, we found that the best parameterization of the model space is mostly three to four layers over a half-space; where the shear-wave velocity of the uppermost layers can follow uniform or power-law dependence with depth. The shear-wave velocity profiles derived by inversion agree with shear-wave velocity profiles provided by borehole surveys at approximately 80% of the sites.

### INTRODUCTION

Surface-wave methods are commonly used in geotechnical engineering to estimate the shear-wave velocity ( $V_S$ ) profile, a key parameter for site characterization. Near-surface analyses usual-

ly combine passive and active sources recorded by multiple receivers deployed in 1D or 2D array configurations. In an ideal context, surface-wave methods allow deriving a  $V_S$  profile comparable to the one obtained from borehole methods (Liu et al., 2000; Brown et al., 2002; Xia et al., 2002; Boore and Asten, 2008) at shallow depth.

Manuscript received by the Editor 18 March 2011; revised manuscript received 5 January 2012; published online 2 May 2012.

<sup>1</sup>Istituto Nazionale di Geofisica e Vulcanologia, Rome, Italy; Institute of Engineering Seismology & Earthquake Engineering, EPPO-ITSAK, Thessaloniki, Greece. E-mail: giuseppe.digiulio@ingv.it.

<sup>2</sup>Institute of Engineering Seismology & Earthquake Engineering, EPPO-ITSAK, Thessaloniki, Greece. E-mail: alekos@itsak.gr; ntho@itsak.gr.

<sup>3</sup>University of Potsdam, Institute of Earth and Environmental Science, Potsdam, Germany. E-mail: mao@geo.uni-potsdam.de; brigitte.endrun@geo.uni-potsdam.de.

<sup>4</sup>Université Joseph Fourier, Institut des Sciences de la Terre, Grenoble, France. E-mail: marc.wathelet@obs.ujf-grenoble.fr; Cecile.Cornou@obs.ujf-grenoble.fr; florence.renalier@obs.ujf-grenoble.fr; pierre-yves.bard@obs.ujf-grenoble.fr.

© 2012 Society of Exploration Geophysicists. All rights reserved.

In the last decades, the use of seismic ambient vibrations as a passive source has gained interest in microzonation studies, due to the accessibility and practicability of collecting field data in urban areas. Ambient vibration measurements are typically recorded by a single station or by temporary 2D arrays of seismological stations (Bard et al., 2010).

The single-station technique is based on the spectral ratio between the horizontal and vertical components of ambient noise (H/V) (Nogoshi and Igarashi, 1971; Nakamura, 1989). The H/V spectral ratio provides good approximation of the resonance frequency  $f_0$  of soft layers, which is, for 1D structures, closely related to the thickness and the velocity of the soft layers (e.g., Lermo and Chavez-Garcia, 1993; Lachet and Bard, 1994; Haghshenas et al., 2008; Castellaro and Mulargia, 2009).

The 2D array techniques based on seismic vibration measurements can complement the information on soil structure provided by the H/V ratios. The two main processing techniques of array methods are the frequency-wavenumber ( $f$ - $k$ ) and the spatial autocorrelation (SPAC) methods. The  $f$ - $k$  method provides the propagation characteristics (i.e., apparent surface-wave phase velocity and azimuth) of waves traveling across the array and includes conventional beamforming (Lacoss et al., 1969; Kvaerna and Ringdahl, 1986) and high-resolution  $f$ - $k$  (Capon, 1969). Both  $f$ - $k$  estimators perform a grid search in the wavenumber plane ( $k_x$ ,  $k_y$ ) through a sliding time-window analysis of filtered data in narrow frequency bands. The SPAC method, as originally proposed by Aki (1957), assumes the wavefield is stochastic and stationary both in space and time. Averaged spatial autocorrelation curves, also termed spatially averaged coherency spectra (Asten, 2006a), are found to be in the form of a Bessel function of zero order (Aki, 1957), the inversion of which allows us to retrieve the Rayleigh phase velocity. The SPAC methodology has been improved in the modified spatial autocorrelation method (MSPAC) to interpret arrays of irregular 2D geometries (Bettig et al., 2001). SPAC applied to the three components of the signal (3C-MSPAC) (Okada and Matsushima, 1989; Chouet et al., 1998; Köhler et al., 2007) is able to utilize both the Rayleigh and Love wave components in the ambient noise wavefield, providing further constraint on the  $V_S$  profile. Further improvements in solving the nonlinear system of equations within the SPAC theory and issues on practical methodology are presented by Cho et al. (2006), Garcia-Jerez et al. (2008), and Tada et al. (2009).

The basic assumption of surface-wave methods applied to ambient vibrations is that the microtremors field is predominantly composed of Rayleigh and Love waves. This assumption cannot be fully met in very stiff sites where a low-energetic contribution of surface waves is possible. Moreover, in urban areas, the ambient noise wavefield can be biased by strong cultural activities (Cara et al., 2010). Endrun et al. (2010) also observe differences in the spectral peaks and in the location of dominant sources at many European sites (some of them considered in the present study) where measurements were repeated at different times. In spite of the discrepancies observed in spectra, they show that surface-wave dispersion and autocorrelation curves are very consistent and stable in time.

A significant amount of research has also been devoted to the joint estimation of phase-velocity dispersion combining passive and multichannel active techniques (Asten and Boore, 2005; Stephenson et al., 2005; Richwalski et al. 2007; Foti et al., 2011). An integrated approach combining active and passive

sources may provide a more accurate phase-velocity dispersion curve. Ambient vibration array methods usually give information on surface-wave dispersion at low frequencies ( $\sim < 5$  Hz), whereas active methods based on a multichannel analysis of surface waves (MASW) (Park et al., 1999) using simple shot sources can increase the accuracy of the dispersion measurements at higher frequency. A joint inversion of phase-velocity dispersion and the H/V curve is also frequently used in geotechnical applications to retrieve a  $V_S$  profile (Scherbaum et al., 2003; Parolai et al., 2005; Fäh et al., 2009), with the H/V curve theoretically related to the Rayleigh wave ellipticity of the fundamental mode (Fäh et al., 2001; Malischewsky and Scherbaum, 2004; Bonnefoy-Claudet et al., 2006; Hobiger et al., 2009).

The recent Network of Research Infrastructures for European Seismology (NERIES EC-Project), Task JRA4 ([www.neries-eu.org](http://www.neries-eu.org)) has been focused on geotechnical characterization of European strong-motion sites and broadband stations (Bard et al., 2010). A goal of the research activity was to develop reliable and low-cost tools based on surface-wave techniques aimed to derive quantitative information on site amplification. One delicate issue related to surface-wave techniques is the inversion of dispersion curves, which is a step independent of the analysis methods and of the sources used for retrieving a dispersion curve. Indeed in the inversion of dispersion curves, one faces a nonlinear and non-unique relation between ground model parameters and observations. An international blind test focused on the inversion of observed and synthetic dispersion curves (Cornou et al., 2006) has shown significant differences in  $V_S$  profiles obtained by different and independent groups of researchers. A large proportion of these discrepancies may be attributed to the inversion process, especially when independent information on near-surface properties cannot be used as constraint in the inversion. The final results of an inversion are strongly affected — in addition to the performance of the inversion algorithm — by the initial assumptions on the parameterization of the model space (Foti et al., 2009; Renalier et al., 2010; Socco et al., 2010) in terms of number of layers, range of velocities and depths, velocity-depth law, Poisson's ratio, and density allowed within each layer. The goal of an inversion process is not strictly the choice of a single best-fitting model, but the selection of a best set of inverted models matching the field observations. A further difficulty in the inversion process is determining how to select the preferred model among a set of competing models that are almost equivalent in terms of misfit, where misfit indicates the discrepancies between observed and theoretical dispersion.

We address the following issues in this paper: (1) how to explore the influence of the parameterization of the model space, (2) what is the most representative parameterization if any, and (3) how to perform a ranking of the models. We analyze the surface-wave dispersion curves measured at 14 European strong-motion sites within Task JRA4 of NERIES EC-Project (Bard et al., 2010). We invert the dispersion curves exploring the model space through a multiple-model parameterization (Savvaidis et al., 2009) composed of four distinct classes. Many resulting models explain satisfactorily the experimental data related to the nonuniqueness problem of the surface-wave inversion. We adopt corrected Akaike's information criterion (AICc) (Akaike, 1973) to quantitatively rank models produced by the inversions. Following this approach, the models with the lowest value of the Akaike estimator (AICc) are considered

as preferred models. We finally compare the  $V_S$  profile obtained by our inversion strategy with the available information at the strong-motion sites. It should be noted that estimators other than the AICc for model complexity or bias correction are presented by (Anraku, 1999; Kuiper et al., 2011; ). Further, the AICc could be also adapted for a Bayesian approach (Akaike, 1980; Burnham and Anderson, 2004; van Erven et al., 2008).

### ESTIMATION OF DISPERSION CURVES AT NERIES SITES

Among the NERIES strong-motion stations (Picozzi et al., 2007; Endrun and Renalier, 2008; Bard et al., 2010), we discard four sites where the measurements with active and passive methods provided do not overlap dispersion curves in a large frequency band (as reported in Renalier and Endrun, 2009). Table 1 gives a description of the selected sites. Table 1 also includes the site classification according to the prescriptions of Eurocode 8 (EC8) building code (CEN, 2004) that is mainly based on the average shear-wave velocity of the topmost 30 m ( $V_{S30}$ ). The near-surface  $V_S$  profiles are derived from available borehole data (downhole or crosshole surveys), except for the three Turkish sites (Bolu, Düzce, and Sakarya) where they are derived from independent MASW measurements (Sandikkaya et al., 2010). The sites show a wide range in terms of expected soil condition, bedrock depth, and environmental conditions (six rural sites and eight urban sites). “Shallow” in Table 1 refers to sites with bedrock depth estimated

from independent information of less than 30 m, “intermediate” sites with bedrock depth varying from 30 to 100 m, and “deep” sites with a bedrock depth more than 100 m. “Unknown” bedrock depth in Table 1 means that available surveys did not reach the bedrock, indicating that its interface lies deeper than 30 m. The variability of the soil structure among sites is also evidenced by the  $f_0$  deduced by the peak of the observed H/V noise spectral ratios varying from 0.4 to 6 Hz (Table 1). However, the  $f_0$  estimate is questionable at some stations because no clear peak is found on the H/V curves. The dispersion curves at each site of Table 1 have been measured for Rayleigh and Love waves during the NERIES project combining ambient vibration array measurements and active seismic surveys;  $f-k$  and SPAC methods have been used to process the data (Renalier and Endrun, 2009; Endrun et al., 2010). Ambient vibration arrays consisted of several (from three to four) small 2D arrays of 3C seismological sensors successively deployed adopting a circular geometry. The array aperture was adapted and increased to sample from short to long wavelength ranges, ranging typically from few meters to several hundred meters. Actual array sizes and station placement are given in Picozzi et al. (2007) and in Endrun and Renalier (2008). Active seismic experiments (MASW) used a simple active source (5 kg hammer) and consisted of a 1D linear configuration of 24 geophones equally spaced between 1 and 5 m, typically using vertical and horizontal 4.5 Hz geophones. In this paper, we do not consider a direct inversion of the autocorrelation curves in the coherency space (Asten et al., 2002, 2006a;

**Table 1. List of the sites analyzed in this article. The site classification follows the Eurocode8 prescriptions, in which  $f_0$  shows the resonance frequency,  $\lambda_{\min}$  and  $\lambda_{\max}$  indicate the minimum and maximum wavelengths given by apparent velocities and frequencies measured directly on the experimental dispersion curves. The association of modes and the difference in percentage ( $\Delta V_{S30}$ ) between  $V_{S30}$  from independent information and from inversion are shown. The estimated  $V_{S30}$  from inversion is computed as average over the 100 best-fitting models (i.e., inverted models at lowest misfit within the best model parameterization).**

Soil class (EC8 code)	Site name and Bedrock depth	$f_0$ (Hz)	$\lambda_{\min} / 3$ / $\lambda_{\max} / 3$ (m)	Modes	$V_{S30}$ (independent information) (m/s)	$V_{S30}$ (from inversion) (m/s)	$\Delta V_{S30}$ (%)
Class B ( $360 < V_{S30} < 800$ m/s)	Aigio (shallow)	6	2-84	R0 L0 L1	540	545	-1
	Norcia (deep)	1	1-196	R0 R1R2 L0	680	440	35
	Sakarya (unknown)	0.8	1-171	R1 L0	400	449	-12
	Sturno (shallow)	0.4	1-306	R0 R1 L0	390	385	1
Class C ( $180 < V_{S30} < 360$ m/s)	Bolu (unknown)	0.7	1-157	R0 L0	280	283	-1
	Buia (intermediate)	not clear	1-124	R1 L0	260	302	-16
	Düzce (unknown)	0.8	1-111	R0 L0	280	293	-5
	Forlì (intermediate)	2	1-199	R0 R1 L0	300	301	0
	Nestos (intermediate)	1.3	1-194	R0 L0	250	207	17
Class D ( $V_{S30} < 180$ m/s)	Volvi (deep)	0.7	2-750	R0 L0	200	234	-17
	Colfiorito Loc1	0.9-1.2	5-35	R0 L2		190	-27
	Colfiorito Loc2 (intermediate)	0.7	1-187	R0 L0	150	133	11
Class E	Knidi (shallow)	6	2-244	R0 L0	707	659	7
	Low-velocity zone	Benevento (deep)	0.4 not clear	1-149	R0 L0		383 (no LVZ)
				R0 R1 L0	740	710 (with LVZ)	4
Korinthos (unknown)		0.5	1-101	R0 L0 L1 R0 L0 L1	340/360	374 (no LVZ) 335 (LVZ)	-7 4

Wathelet et al., 2005). Instead, we prefer to consider only surface-wave dispersion curves in the inversion. Rayleigh wave dispersion curves are derived from  $f$ - $k$  and MSPAC analysis of vertical components of seismic signals. Love wave dispersion curves are assessed by 3C-MSPAC analysis on ambient vibrations and by  $f$ - $k$  analysis on the horizontal components of the signals collected by MASW surveys. We include in the inversion process higher modes when they are clearly observed after a visual inspection of the experimental curves. The association of modes to the experimental curves is indicated in Table 1 (R and L are Rayleigh and Love waves; R0, R1, and R2 are fundamental, first and second higher mode of Rayleigh waves, respectively).

Mean Rayleigh and Love dispersion curves are obtained at the selected sites by averaging the dispersion curves estimated with the different array methods. As an example, Figure 1 displays the Rayleigh and Love dispersion curves at the Nestos site, including the dispersion curves theoretically computed from the velocity structure (Dunkin, 1965; Herrmann, 1987) obtained by available refraction and crosshole data. We prefer to show the surface-wave

dispersion curves in the frequency-slowness domain; slowness (reciprocal of velocity) gives a better representation than velocity of the near-surface materials that amplify the local ground motions (Brown et al., 2002; Boore and Asten, 2008). The main discrepancies are observed for the theoretical dispersion curves computed on the crosshole profile (yellow curves in Figure 1a and 1b). The crosshole model provides lower slowness in all analyzed frequency bands; the reason may be lateral variations of velocity in the very topmost layer (the distance between the crosshole location and the center of 2D arrays is about 200 m at this site). The dispersion curve from the refraction model agrees with MASW results approximately in the range of 5–50 Hz (Figure 1a and 1b). The MASW surveys provide surface-wave information in the high-frequency range ( $\sim > 5$  Hz) due to the limited frequency content of the seismic signal generated by the active source (5 kg hammer) at longer periods. The surface-wave dispersion curves derived from ambient vibration data cover also the low-frequency range (approximately up to 1 Hz), where the active methods do not provide information (Figure 1a and 1b). At low-frequencies ( $< 2$  Hz), the MSPAC Rayleigh curve shows higher slowness than the one derived by the  $f$ - $k$  method (Figure 1a). A similar difference between  $f$ - $k$  and MSPAC is systematically observed in the low-frequencies range at the investigated sites. This is explained in terms of a better resolution at long periods of MSPAC than  $f$ - $k$  methods, as already highlighted by many authors using real data and simulations (Othori et al., 2002; Cho et al., 2004; Wathelet et al., 2008; Clapgood and Asten, 2009). Deviation between  $f$ - $k$  and MSPAC Rayleigh wave curves is also observed at about 10 Hz (Figure 1a), where MSPAC deviates toward lower slowness values, probably indicating a signal contamination caused by body waves or the influence of higher modes (not clearly identified at the Nestos site).

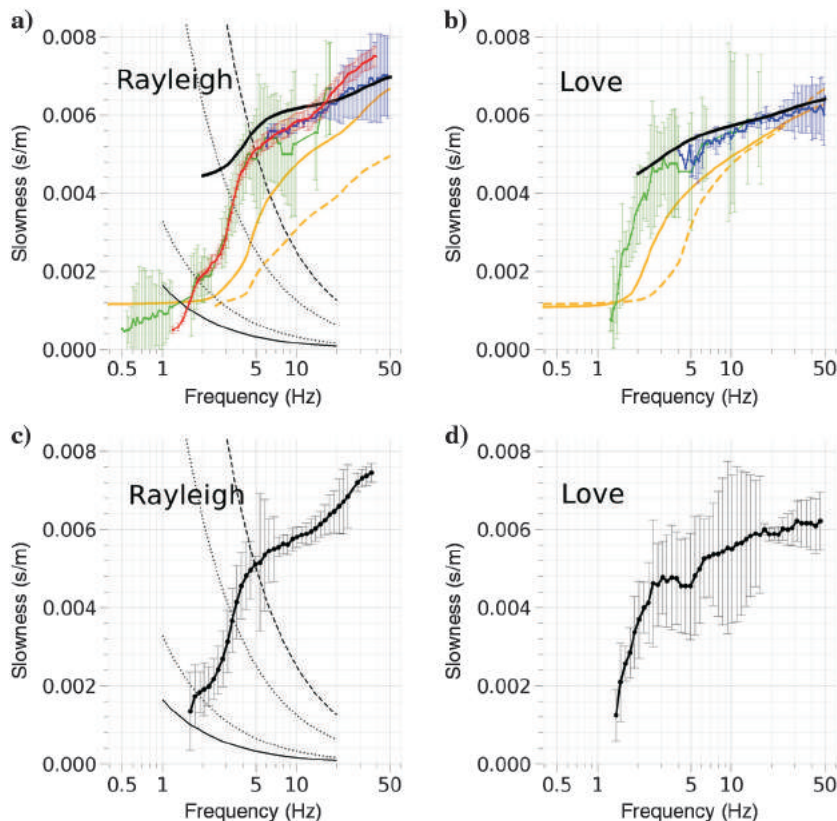


Figure 1. Dispersion curves observed at Nestos site for (a) Rayleigh and (b) Love waves. The green curves in (a and b) are obtained from SPAC analysis on ambient vibrations whereas the blue curve is derived from  $f$ - $k$  analysis of MASW data. The red curve is the average between conventional beamforming and high-resolution  $f$ - $k$  applied on ambient vibrations. The thick black curve in (a and b) show the theoretical dispersion curves computed from  $V_S$  profiles obtained by refraction data. The yellow curves show both the fundamental (continuous curve) and first higher mode (dashed curve) theoretically computed from the crosshole  $V_S$  profile. The thin solid, dashed, and dotted curves in (a and c) show the resolution and aliasing curves as defined in Wathelet et al. (2008) for the largest array deployed at this site. The dispersion curves of (c and d) are used in the inversion and are obtained after selection and averaging of the curves in (a and b).

## MULTIMODEL PARAMETERIZATION

We invert the surface-wave dispersion curves collected at the strong-motion sites of Table 1 exploring extensively the model space parameterization. We apply the neighborhood algorithm (Sambridge, 1999) as implemented by Wathelet (2008) to solve the nonlinear problem of surface-wave inversion of the experimental curves in a multidimensional parameter space. The neighborhood algorithm is a direct search method using Voronoi cells to investigate the model space and generating iteratively new random models inside the most promising cells.

We evaluate the influence of the parameterization in the inversion analysis through a multimodel parameterization. We consider four distinct classes of parameterizations of the model space. We first use uniform layers with constant velocity over the half-space; this is probably the most simple and diffuse parameterization in the inversion analysis of surface-wave dispersion. We then

consider models with gradually increasing ground stiffness with depth; the velocity-depth function follows a power-law or linear-law dependence. This typology of parameterization is designed for reproducing the compaction of subsoil with depth in sedimentary environments (Ibs-von Seht and Jürgen, 1999; Parolai et al., 2002; Boore et al., 2011). The last class of parameterization is based on a geometric progression of the layer's thickness to account for the decrease of resolution with depth.

For each class of parameterization, we progressively increase the number of layers over the half-space. The four parameterization groups are indicated as UF, 1PL, 1L, and GP (Table 2) and are designed in detail as follows:

- UF — uniform layering allowing a number from one to nine homogeneous layers over the half-space.
- 1PL — a topmost layer composed of five sublayers with the velocity-depth function exhibiting power-law dependence. The  $V_S$  at depth  $z$  is given in the general form  $V_S(z) = V_{S0}(1 + z - z_0)^\alpha$ , where  $z_0$  indicates the depth of the top of the layer (i.e., here, for the topmost layer:  $z_0 = 0$ ) and  $V_{S0}$  is the velocity at depth  $z_0$ . There are then three independent parameters for the inversion:  $z - z_0$ ,  $V_{S0}$ , and  $\alpha$  for this topmost layer, which is overlaying a number from one to eight uniform layers with constant velocity over the half-space.
- 1L — a topmost layer composed of five sublayers with the velocity-depth function following a linear law (i.e.,  $\alpha = 1$  in the above equation). The topmost layer is underlaid by one to eight uniform layers over the half-space.
- GP — similar to UF but with a distribution of thickness following a geometrical progression ( $z_i = a \cdot b^i$ ).  $z_i$  is the thickness of the  $i$ th layer, the parameter  $a$  is set to a quarter of the minimum measured wavelength, the parameter  $b$  is given by the constraint that the sum of  $z_i$  for all layers is half of the maximum measured wavelength. This particular distribution of thickness is chosen to increase the penetration depth.

The four parameterization groups define the 1D tabular ground structures used for the theoretical computation of surface-wave dispersion curves. Increasing the number of layers into the UF, 1PL, 1L, and GP parameterizations means increasing the number of degrees of freedom (DOF) describing the model space in the inversion

analysis of dispersion curves. The DOF of the model space of the four parameterizations ranges from five to 31 (Table 2), assuming the DOF as the number of free (adjustable) parameters into the parameter space. The free parameters to consider in the description of each elastic layer are the  $V_S$ , the compressional velocity  $V_P$ , and the thickness. We decided to fix the density to  $2 \text{ g/cm}^3$  because of the low sensitivity of surface-wave dispersion to this parameter (Xia et al., 1999). The  $V_P$  profiles are characterized by the same four classes of parameterization as the  $V_S$  profiles, with the  $V_P$  values linked to the  $V_S$  values through the Poisson's ratio. Because we do not have information on the water table depth, we fix the  $V_P$  interface to be at the same depth as each corresponding  $V_S$  interface. These assumptions on the  $V_P$  represent a good compromise for the inversion process to obtain reliable solutions without increasing excessively the number of DOF.

We allow a large range of possible values for the free parameters during the inversion: the search interval of  $V_S$  ranges from 50 to 2500 m/s, and from 150 to 3500 m/s for the half-space. The search interval of  $V_P$  is from 200 to 5000 m/s, with the  $V_P/V_S$  ratio related to the Poisson's ratio. The Poisson's ratio is not a parameter of the inversion like  $V_P$  or  $V_S$ , and it is forced to be inside a specified large range (0.2–0.5) for all layers of the generated models. The thickness limits are defined into the four classes of parameterization by using the measured wavelengths  $\lambda$  from the observed dispersion curves. In the first three parameterization groups, the boundaries of all layers were constrained within the limits  $\lambda \text{ min}/3$  and  $\lambda \text{ max}/3$ , where  $\lambda \text{ min}$  and  $\lambda \text{ max}$  are the minimum and the maximum measured wavelengths at the investigated sites (see Table 1). The rule in estimating the penetration depth of surface waves as  $\lambda/3$  is empirically adopted and supported by the results of the NERIES EC-Project (deliverable JRA4-D6). However, the loss of resolution with depth of surface waves is dependent on the structural model and soil properties. The fourth parameterization (GP) is designed to increase the penetration depth more than the UF, 1L, and 1PL classes. The thickness of the first layer is fixed to  $\lambda \text{ min}/4$  and the maximum investigation depth for the deepest layer to  $\lambda \text{ max}/2$ .

The tuning parameters of the neighborhood algorithm are the initial number of models  $n_{s0}$ , the number of new models  $n_s$ , and the number of cells  $n_r$ . A misfit function is first computed for the initial set of  $n_{s0}$  models. Within the  $n_r$  cells with the lowest misfit, a total of  $n_s$  new models are added ( $n_s/n_r$  samples generated per cell). The last two steps are repeated  $N$  times, resulting in a total of  $n_{s0} + N \times$

**Table 2. DOF associated with each model parameterization. UF, 1PL, 1L, and GP indicate the four parameterization groups described in the text. The last number in the names of model parameterizations indicates the number of uniform layers over the half-space. Example of DOF computation in the 1L\_1 case: We have a topmost layer with a linear velocity law described by five free parameters (its total thickness and the  $V_P$  and  $V_S$  at the top and at the bottom of this layer) overlaying a uniform layer, which is described by further three free parameters ( $V_P$ ,  $V_S$ , and thickness). Additional two free parameters are the  $V_P$  and  $V_S$  of the half-space.**

Model parameterization	UF_1	GP_1	UF_2	GP_2	UF_3	GP_3	UF_4	GP_4	UF_5	GP_5	UF_6	GP_6	UF_7	GP_7	UF_8	GP_8	UF_9	GP_9
DOF	5		8		11		14		17		20		23		26		29	
Model parameterization	1L_1	1PL_1	1L_2	1PL_2	1L_3	1PL_3	1L_4	1PL_4	1L_5	1PL_5	1L_6	1PL_6	1L_7	1PL_7	1L_8	1PL_8		
DOF	10		13		16		19		22		25		28		31			

$n_s$  models. We use  $n_{s0} = 100$ ,  $n_s = 50$ ,  $n_r = 50$ , and  $N = 4000$  resulting in a total of 200,100 models. We repeat five runs (with five different random seeds) for each set of selected parameterizations to test the robustness of the results.

The misfit measure  $m$  between observed and theoretical dispersion curves is computed for each inverted model and is defined as

$$m = \sqrt{\sum_{i=0}^{n_f} \frac{(x_{di} - x_{ci})^2}{\sigma_i^2 \cdot n_f}}, \quad (1)$$

where  $x_{di}$  and  $x_{ci}$  are the phase velocity of observed and theoretical dispersion at frequency  $f_i$ , respectively. The standard deviation is  $\sigma_i$  at frequency  $i$ , and  $n_f$  is the total number of samples. During the analysis process, the data are filtered in narrow frequency bands (100–150 frequency bands) fixing the time-window length as 50–80 times the central period of the analyzed frequency band. This choice with an overlap of 5% provided experimental curves averaged over many windows at fixed frequencies, allowing the statistical computation of standard deviations.

Figure 2c displays the typical behavior of the misfit with an increasing number of layers in the model space parameterization, and Figure 2a shows that 200,100 inverted models are enough to reach the plateau branch of the misfit trend.

For the sake of simplicity, we do not allow the presence of low-velocity zones (LVZ) in the inversion process except at two sites (Benevento and Korinthos), where borehole data strongly suggest shear-wave velocity reversal in the  $V_S$  profiles. For all the sites, we deliberately do not introduce constraint from borehole data or from the observed  $f_0$  during the inversion. Borehole data and  $f_0$  from the H/V curves are considered as a priori information, and they are used for comparison with the models resulting from inversion. The Dinver package within the Geopsy tool ([www.geopsy.org](http://www.geopsy.org)) is used for the modal surface-wave inversion.

### MODEL RANKING BASED ON AKAIKE'S INFORMATION CRITERION

The multimodel parameterization with an extensive inversion produces a large number of models showing similar values of misfit (equation 1 and Figure 2a). Each parameterization class is then characterized by a different number of DOF (Table 2) describing the model space. For the identification of a best class of fitting models among an ensemble of acceptable models, we use the Akaike information criterion (AIC). Akaike's idea is to relate the Kullback-Leibler information number, which indicates the information lost when an approximating model is used to explain reality, to the maximum likelihood function (Kullback and Leibler, 1951; Akaike, 1973, 1974;

Bozdogan, 2000). The AIC estimator combines the maximized likelihood and the number of free parameters  $K$  within the model through the general form

$$\text{AIC} = -2 \cdot \ln(\text{maximum likelihood}) + 2 \cdot K, \quad (2)$$

where  $\ln$  indicates the natural logarithm. The first term of equation 2 is a measure of the lack of fit between the approximating model and the true model representing the reality; the second term of equation 2 penalizes the model complexity. This is consistent with the principle of parsimony that investigates the number of free parameters of possible approximating models to reach the best compromise between bias and variance. Models with a lower value of AIC are considered to be better models. AIC or similar information-theoretic approaches do not require particular assumptions on the experimental data and they are used for problems of model decision in various fields of environmental, hydrology, and numerical analyses (Mutua, 1994; Burnham and Anderson, 2001; Zhao et al., 2008). A seismic application is presented by Boore and Thompson (2007), who used AIC in near-surface analysis focusing on the selection of the interface depths from the inversion of seismic traveltimes. Savvaidis et al.

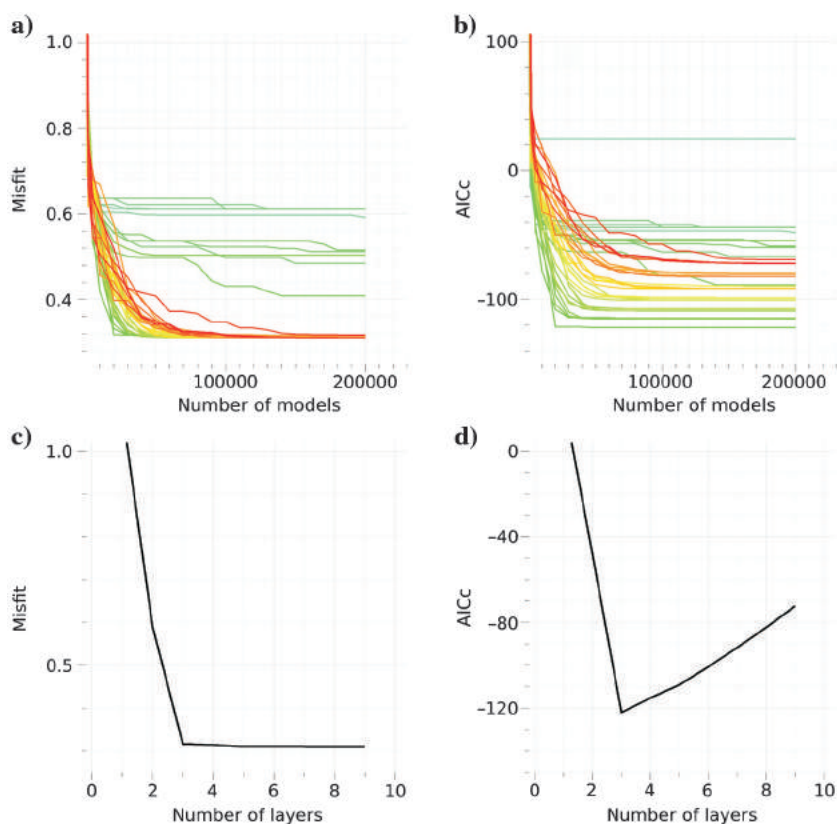


Figure 2. (a) Misfit and (b) AICc evolution versus number of models. The example is for the Aigio site using a uniform model space parameterization (UF of Table 2). The color scale of curves refers to the number of layers progressively added (from green to red with increasing number of layers). Note that the most complex models (red curves) reach an asymptotic behavior when 200,100 models are produced. (c) Misfit and (d) AICc versus number of layers progressively added in the model parameterization (UF parameterization and the Aigio site).

(2009) apply AIC in the inversion analysis of a theoretical dispersion curve.

In case of least-squares estimation with normally distributed errors and for small sample sizes, Sugiura (1978) and Hurvich and Tsai (1989) propose a corrected version of equation 2 expressed as

$$\text{AICc} = n_f \cdot \ln(\hat{e}^2) + 2K + (2K(K + 1)/(n_f - K - 1)), \quad (3)$$

where  $n_f$  is the total number of observations and  $\hat{e}^2$  is the sum of the estimated residuals for the candidate models divided by  $n_f$ . In our application,  $\hat{e}^2$  corresponds to the misfit  $m$  defined by equation 1,  $n_f$  is the number of samples of the experimental dispersion curves, and  $K$  indicates the DOF of each considered model parameterization (listed in Table 2).

## RESULTS

At each site of Table 1, we first invert the surface-wave dispersion curves using the four classes of parameterization of the model space. Then we follow the Akaike criterion to extract a best set of fitting models resulting from the inversion. Within each parameterization class, we group the results of the five inversion runs (i.e., five seeds) by computing the AICc value through equation 3. We then plot the evolution of the AICc as a function of the DOF (or in other words, as a function of the number of layers progressively added over the half-space) (Table 2). Figure 2b and 2d shows the general trend of AICc when varying the number of inverted models and the number of degrees of freedom, respectively. AICc usually converges toward a clear minimum for a given number of DOF (Figure 2d). We select as best model parameterization the one showing the minimum of the AICc number (Figure 2d). Note that the lowest AICc number (equation 3) does not necessarily correspond to the lowest absolute misfit (equation 1). In the following, we show the inversion results according to the best model parameterization selected by the Akaike approach. The models with lower misfit into this best model parameterization are selected as the most representative models. Finally, we compare the best set of models resulting from our inversion strategy with the a priori information (i.e., available  $V_S$  profiles and H/V noise spectral ratios).

We also compare the  $V_S30$  derived from inversion with the  $V_S30$  estimated by independent information. For simplicity, we group the sites following the EC8 soil classification based on  $V_S30$  values (see Table 1). The main aim of our inversion procedure is not the  $V_S30$  estimation, which may be satisfactorily assessed at the selected sites by the observed phase velocity at a given wavelength (Renalier and Endrun, 2009; Bard et al., 2010) or likely by a less intensive inversion. However, the comparison in terms of  $V_S30$  allows us to examine the reliability of the resulting models derived from our inversion strategy, at least for the near-surface velocity (Moss, 2008). Our approach provides an acceptable error in the  $V_S30$  estimates ( $\Delta V_S30$ ) inferior to 20% on average (Table 1).

### STIFF SITES (SOIL CLASS B)

Aigio, Norcia, Sakarya, and Sturno are considered stiff sites based on the available information (Table 1). Following the EC8 code (CEN, 2004), these sites are soil class B (360 <

$V_S30 < 800$  m/s). We consider higher modes in the inversion to increase the reliability of the inverted model (Xia et al., 2003). Energetic higher modes are found on the experimental dispersion curves at all stiff sites and are likely caused by a significant velocity contrast between the shallowest part of the velocity profile and the underlying stiff layers. The best parameterization for the stiff sites is well indicated by the AICc behavior with varying DOF (Figure 3, first column); the lowest AICc is for a model space defined by 13 or 14 DOF (Table 2). The inversion results within this best parameterization of the model space (i.e., parameterization with the lowest AICc number) are also shown in Figure 3. The inversion results provide misfit quite low (<0.4) and fairly acceptable fits between experimental and theoretical dispersion curves for most stiff sites (Figure 3). The shear-wave slowness profiles resulting from the inversions agree best with the reference borehole profiles in the topmost layers (approximately at a depth <20 m), whereas larger discrepancies are observed at a larger depth (depth >20 m). This could be explained by the lack of estimates of phase velocities at low frequency (i.e., < 2 Hz), related to a poor resolution of the array techniques applied to stiff sites in retrieving reliable information on the wavefield at long periods.

In terms of soil classification, the  $V_S30$  derived by a priori information and the  $V_S30$  inferred by inverted models are within the same EC8 class, with Norcia showing the largest discrepancy on  $V_S30$  ( $\Delta V_S30$  of 35%, Table 1). At Norcia, the experimental Love wave curve is not adequately fitted by the inversion above 10 Hz (Figure 3, L0 curve at the second row). The reason of this mismatch at Norcia is unknown. However, surface-wave inversion can provide wrong velocities in cases of departure from the usual assumption of homogeneous 1D layers. Conversely, a borehole survey is indicative of the properties of a subsoil column, and in the presence of lateral heterogeneity of the subsoil it cannot be extrapolated to other areas. The differences between inversion results and a priori information could be also ascribed to wrong mode identification or to the effects of the LVZ (as indicated by the borehole data of Norcia).

In Figure 4, the measured H/V noise spectral ratios (red curves) are compared to the theoretical Rayleigh wave ellipticities (Dunkin, 1965; Tokimatsu, 1997) of the fundamental mode (black curves). The Rayleigh wave ellipticities are computed for the 100 models with the lowest misfit into the best model parameterization indicated by AICc. At Aigio, Norcia, and Sakarya, the ellipticities reproduce fairly well the resonance at high frequencies (about 6–8 Hz) observed in the H/V spectral ratios. In the low-frequency band (<1 Hz), the H/V spectral ratios do not show a distinct peak but a weak amplification (amplitude level <3) that is not reproduced by theoretical ellipticity curves. This is consistent with the difficulty in resolving deep layers at stiff sites from surface-wave methods (Arai and Tokimatsu, 2005; Pileggi et al., 2011; Tuan et al., 2011). Excluding the high-frequency resonance (6–8 Hz), the theoretical ellipticities underestimate the amplitude level of the observed H/V spectral ratio probably related to the contribution of Love or body waves in the horizontal components of the wavefield (Arai and Tokimatsu, 2004).

### SOFT SITES (SOIL CLASS C)

At soft sites (180 <  $V_S30$  < 360 m/s), the match between experimental and inverted dispersion curves is acceptable (misfit <0.4) in

all cases (Figure 5). The reference borehole profiles agree with the inverted profiles, with the large differences observed at Buia. At this site, the experimental dispersion curves are far from the fundamental mode reference curves, and the inversion shown in Figure 5 (second row) is with the Rayleigh curve considered as first higher

mode (R1). The inversion of Buia (Figure 5, second row) indicates a low misfit (about 0.25), but the H/V spectral ratios do not agree with the theoretical ellipticities (Figure 6). The reason of this disagreement is unclear. It may however be related with the complexity of the site, which is situated in a basin of fluvial-glacial deposits with

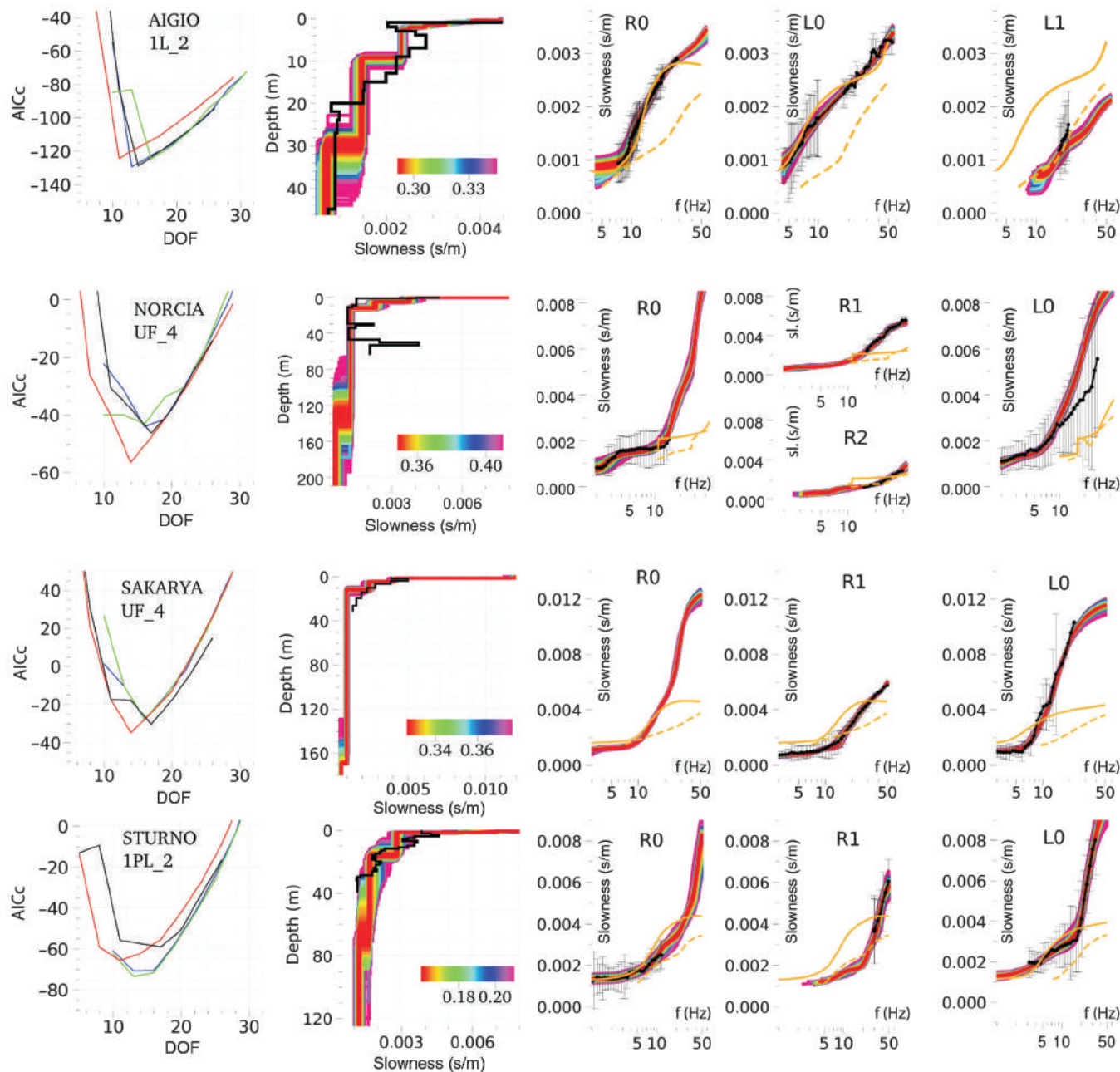


Figure 3. Results at stiff sites (soil class B). The left panel shows the AICc evolution versus the number of DOF. Each colored curve represents one of the four parameterization classes: green, black, blue, and red curves refer to 1PL, GP, 1L, and UF model parameterizations of Table 2. The name of the best model parameterization (i.e., lowest AICc) is indicated below the site name. The remaining panels show the inversion results within the best model parameterization: shear-wave slowness profiles and Rayleigh (R) and Love (L) dispersion curves. The fundamental mode is indicated as R0 (L0), the first higher mode as R1 (L1), and the second higher mode as R2 (L2). The color scale gives the misfit; the misfit scale ranges from the minimum misfit ( $m_{min}$ ) provided by inversion to  $m_{min} + 0.05$ . The black curves within the  $V_S$  profiles and within the dispersion curves show the borehole and the input data, respectively. The orange curves show the forward modeled dispersion (fundamental and first higher mode) resulting from the reference profile.



irregular configuration, and near the fault surface rupture responsible for the largest earthquakes of the region (Fäh et al., 1993; Aoudia et al., 2000). Sandron et al. (2011) conclude that the seismic response of Buia site to strong motion can only be partially explained by standard 1D analyses of vertically propagating SH-waves. A mismatch between H/V ratios and ellipticities is also found at the Forlì site; the theoretical spectral peak of the ellipticities at approximately 1 Hz is not observed on H/V spectral ratios (Figure 6). The 1-Hz peak is related to a bedrock estimated by the best-fitting models at an approximate depth of 200 m (corresponding to  $\lambda_{\max}/3$ , see Table 1), which is outside the resolution capabilities of the array data because our dispersion curves hardly extend below 2 Hz (Figure 5). This lack of resolution is indicated by the unresolved deepest layer of the inverted  $V_S$  models for Forlì. Models with low misfit values (red in Figure 5, fourth row) show a very large variability of  $V_S$  (from 1000 to 3000 m/s) for the basement.

Bolu and Düzce show very similar H/V curves; and the theoretical ellipticities exhibit lower amplitudes than the H/V curves in the entire frequency band (Figure 6). This effect could be related to a low-velocity contrast of the soil structure. The H/V ratios at Nestos and Volvi are characterized by a strong and narrow spectral peak, which frequency agrees very well with the ellipticities of the inverted models (Figure 6), and consistently the  $V_S$  profiles present a strong velocity contrast. Volvi is located in an alluvial basin 6-km long and 200-m deep in northern Greece, and it was selected as a European test site for investigating site effects (<http://euroseis.civil.auth.gr/>). The Volvi basin is a graben structure filled with recent deposits, and geophysical and geotechnical investigations provided the soil layering (Jongmans et al., 1998) allowing reliable numerical modeling (Beuval et al., 2003; Semblat et al., 2005; among many others). The main discrepancy resulting from the inversion at Volvi is on the depth of the basement (Figure 5, sixth row): The sediments-to-bedrock interface is reported by the reference borehole at approximately 200 m (Raptakis et al., 2000), whereas the inverted models yield an interface depth at approximately 130 m deep. The difficulty in resolving the bedrock depth is likely related to a resolution issue caused by very few points of Rayleigh wave dispersion curve below 0.7 Hz with relatively large errors. This frequency corresponds to the  $f_0$  of the site where the energy of vertical motion is vanishing (Fäh et al., 2001).

Additional effects could bias the interpretation of resonance frequencies and then of the bedrock depth in valley environments. The usual assumption of 1D layered geology (and local 1D resonance) within the surface-wave analysis cannot be completely respected in complex geologic structures like deep alluvial basins. Two-dimensional or 3D resonance effects, including a preferential polarization of the microtremor wavefield, are possible in deep

valleys as observed from numerical and experimental studies (Bard and Bouchon, 1985; Roten et al., 2006; Lenti et al., 2009; Clapgood et al., 2011). Chaljub et al. (2009) observe 3D effects in the Volvi basin, comparing numerically simulated earthquake ground motion to experimental data. These authors found an agreement between the  $f_0$  deduced from 3D simulation and the one derived from site-to-reference spectral ratio (with the reference station being installed at a depth of 200 m within the Volvi basin). They found a resulting  $f_0$  showing lower amplitude and shifted toward higher frequency than the  $f_0$  assessed by the 1D transfer function.

### VERY SOFT SITES (SOIL CLASS D)

Colfiorito is the only site in Table 1 that belongs to soil class D ( $V_{S30} < 180$  m/s). The site is within a 3-km-wide intramountain alluvial basin in central Italy, with a complex topography of the buried bedrock responsible for 2D-3D effects on seismic ground motion (Di Giulio et al., 2003). Two locations at Colfiorito (loc1 and loc2, at a distance of about 500 m from one another) are investigated by the NERIES EC-Project (deliverable JRA4-D6). Loc1 and loc2 sites are situated 1000 and 700 m southeast from the available borehole position, respectively. At the first location (loc1) of Colfiorito, a seismic array with very small aperture (about 40 m) was deployed to

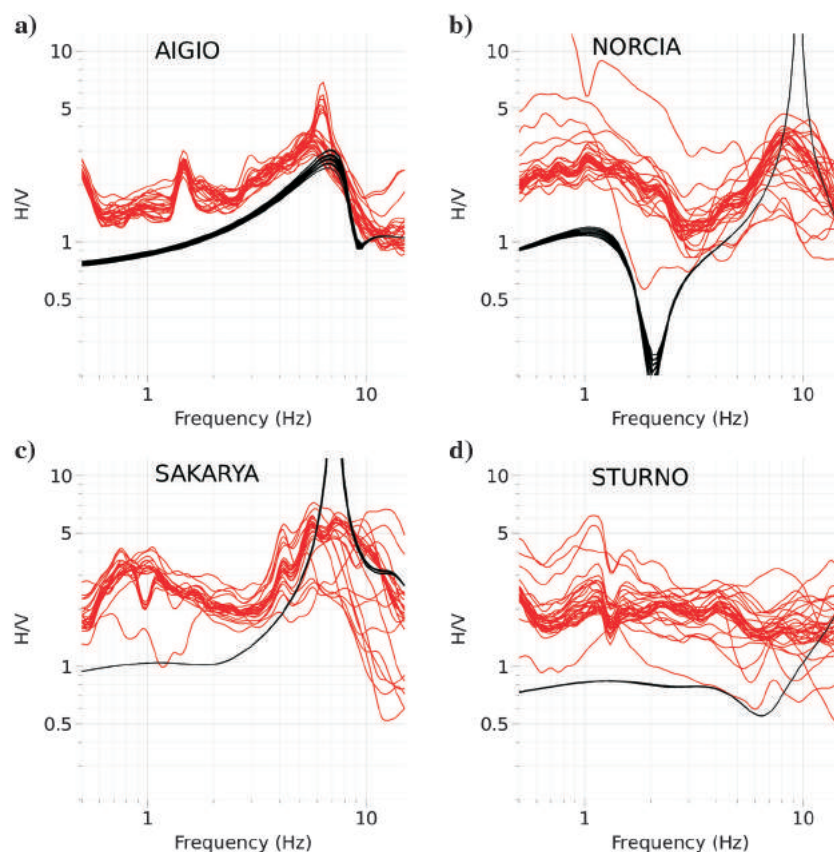


Figure 4. The H/V curves at stiff sites (soil class B). The observed H/V noise spectral ratios (red curves) for all stations of the array are compared to the theoretical Rayleigh wave ellipticities of the fundamental mode (black curves) for the 100 best-fitting models (i.e., lowest misfit within the best model space parameterization indicated by AICc estimator).

record ambient vibrations. The results shown in the top panel of Figure 7 are derived for loc1 by considering the surface-wave measurements as fundamental Rayleigh mode (R0) and second higher mode Love waves (L2). Note that the minimum of AICc corresponds with the lowest number of DOF, indicating a simple structure for the site (a single soft layer over the half-space). The best model parameterization indicated by AICc is the one using the geometric progression

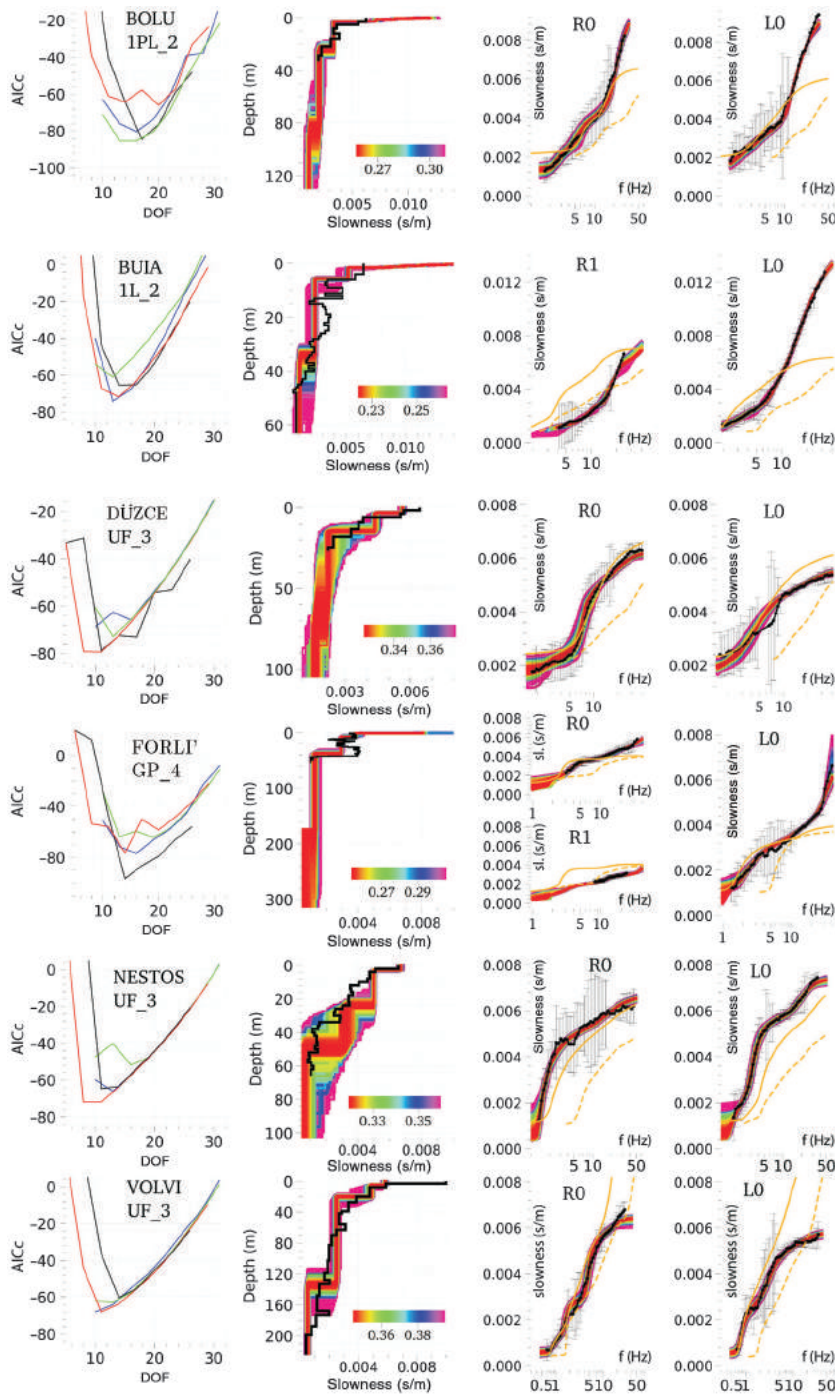


Figure 5. Results at soft sites (soil class C). Graphical schemes follow the description in caption of Figure 3.

(GP). Although the GP parameterization is related to a larger investigation depth than the one allowed in the other three parameterization groups ( $\lambda \max/2$  versus  $\lambda \max/3$ , respectively), the velocity of the bottom basement is not resolved by the inversion (Figure 7), probably due to the small aperture of the arrays (maximum aperture of about 40 m). The borehole profile available at Colfiorito shows higher shear-wave slowness and a deeper interface than the models

resulting from the inversion at the loc1 site (Figure 7). The discrepancy in  $V_{S30}$  between borehole and inversion results (150 versus 190 m/s, Table 1) leads to a different EC8 soil classification (from class D to class C). The difference at loc1 site in both velocity ( $\Delta V_{S30}$  of 27%, Table 1) and depth of interface can be explained by taking into account lateral heterogeneities between the available borehole and the position (loc1) of the array. Near the edge of the basin, higher-velocity superficial layers composed of alluvial fans are present (Di Giulio et al., 2006). The borehole is located approximately in the central part of the basin where the  $f_0$  is 0.9 Hz as computed from H/V ratios of previous experiments, whereas loc1 array is located 600 m away from the southeast edge of the basin edge. Two multiple peaks with similar amplitude can be recognized on the observed H/V curves at the loc1 site (at 0.9 and 1.2 Hz; see Figure 7). The former frequency corresponds to the  $f_0$  interpreted by microtremor measurement in proximity of the borehole. The inversion at loc1 is not able to reproduce such complexity related to multiple peaks; the theoretical ellipticity of fundamental Rayleigh wave evaluated from the inverted models shows a peak at an intermediate frequency (approximately 1 Hz, Figure 7).

At the second location of Colfiorito (loc2), the inversion (in terms of fundamental modes R0 and L0, see Figure 7) shows a better agreement for the  $V_{S30}$  (Table 1) but a larger depth of the sediment-to-bedrock interface than the borehole profile (70 m versus 55 m, respectively). Similarly to the loc1 site, the difference in the bedrock depth can be explained in terms of lateral heterogeneity of the geologic structure between the borehole position and the loc2 array position. A deeper bedrock at loc2 provided by inversion is consistent with the different values of  $f_0$ ; 0.7 Hz is computed at loc2 from the H/V curves (Figure 7), whereas 0.9 Hz was measured at the borehole location.

## SITE OF CLASS E

The borehole profile characterizes Knidi as a stiff site ( $V_{S30}$  of 707 m/s) with superficial soft sediments of less than 20-m thickness over a very stiff basement, as prescribed by EC8 for soil class E. The inversion at Knidi (Figure 8) shows very high misfit values ( $m > 1$ ) because

the high-frequency portion ( $f > 20$  Hz) of experimental R0 is not matched by the inversion. Nevertheless, the inversion provides  $V_S$  profile and thickness of the soft layer, which agrees fairly well with the borehole profile. The theoretical ellipticities slightly overestimate the frequency of the strong peak obtained at approximately 6 Hz by the H/V spectral ratios (Figure 8). This difference on the  $f_0$  can be linked to a not fully valid 1D assumption within the surface-wave analysis. Figure 8 shows a spatial variability of the H/V curves among the array stations. This array was deployed on a hill very close to the strong-motion site characterized by very shallow bedrock. We suspect that topographic effects and/or local lateral variations of the uppermost layer within the array aperture are responsible for the variability of the H/V measurements.

### EFFECTS OF LOW-VELOCITY ZONES

We consider the effects of LVZ only at two sites (Benevento and Korinthos) where the available borehole profiles document layers with a significant decrease in velocity with depth (Figure 9). We perform the inversion with and without LVZ at these two sites. In principle, allowing velocity inversions in the model increases the nonuniqueness associated with the inversion of surface-wave dispersion curves (Wathelet et al., 2005). LVZs may produce an irregular shape on the observed dispersion curve and the effects could be misinterpreted as higher modes. In addition to the velocity contrast, the

effect of an LVZ is related to its depth and thickness. The sensitivity of Rayleigh wave dispersion curves is low for the layers below the LVZ (Cercato et al., 2010), leading to poor resolution for the layers underlying LVZ. Asten (2006b) shows a successful case in resolving LVZ through a direct-fitting method of the SPAC curves in the coherency space. Hamimu et al. (2011) suggest a joint inversion of

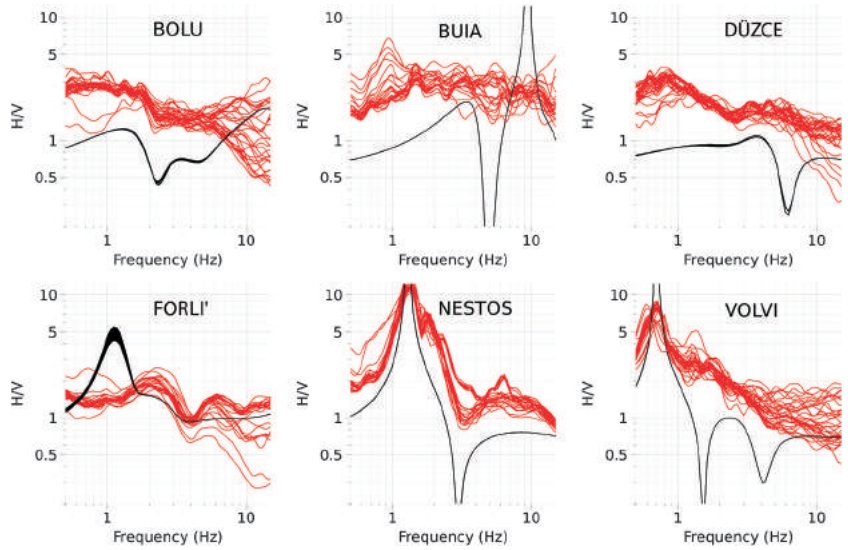


Figure 6. The H/V curves at soft sites (soil class C). The observed H/V noise spectral ratios (red curves) for all stations of the array are compared to the theoretical Rayleigh wave ellipticities of the fundamental mode (black curves) for the 100 best-fitting models (i.e., lowest misfit within the best model space parameterization indicated by AICc estimator).

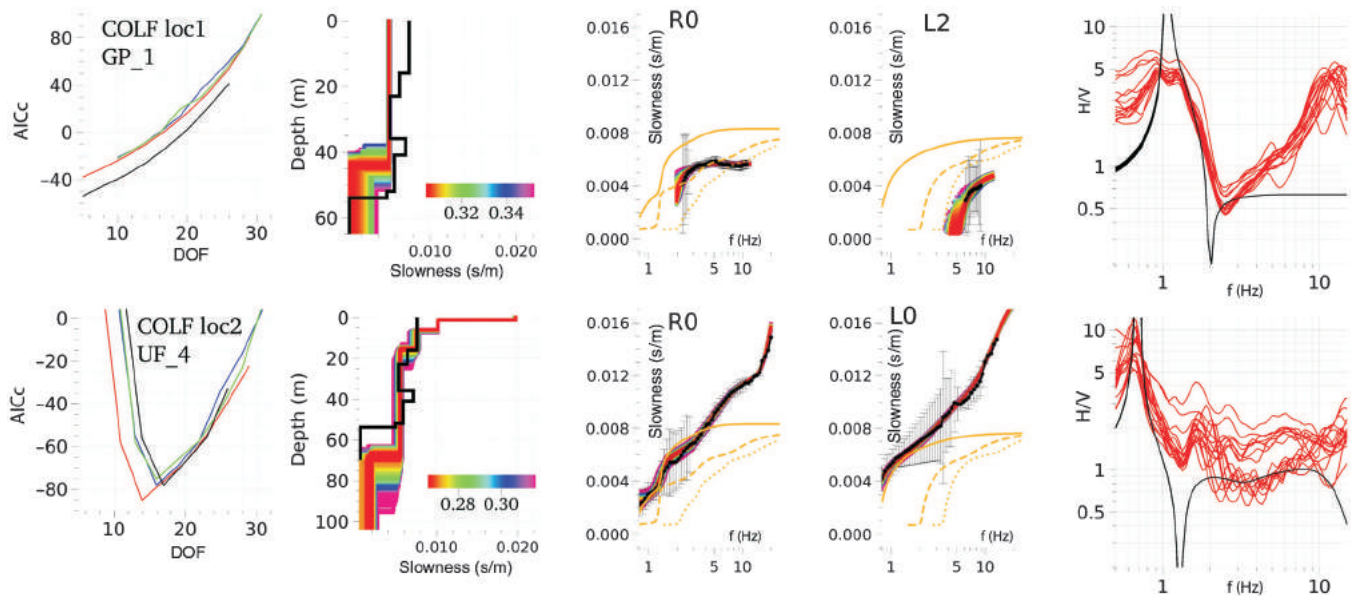


Figure 7. Results at the Colfiorito site (soil class D). The yellow curves show the fundamental (continuous curve) and the first and second higher modes (dashed curve) theoretically computed from the reference  $V_S$  profile. Graphical schemes for AICc, slowness profiles, and dispersion curves are described in the caption of Figure 3. The H/V curves are as described in the caption of Figure 4.

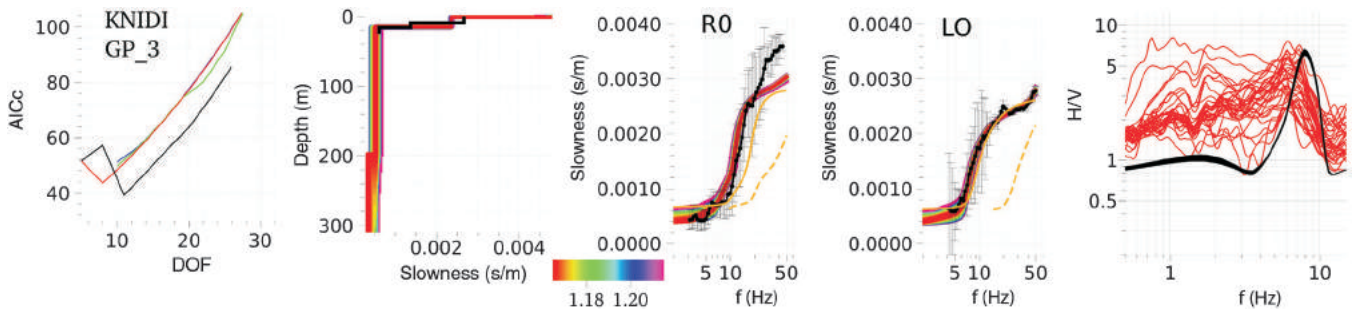


Figure 8. Results at the Knidi site (soil class E). Graphical schemes for AICc, slowness profiles, and dispersion curves are described in the caption of Figure 3. The H/V curves are as described in the caption of Figure 4.

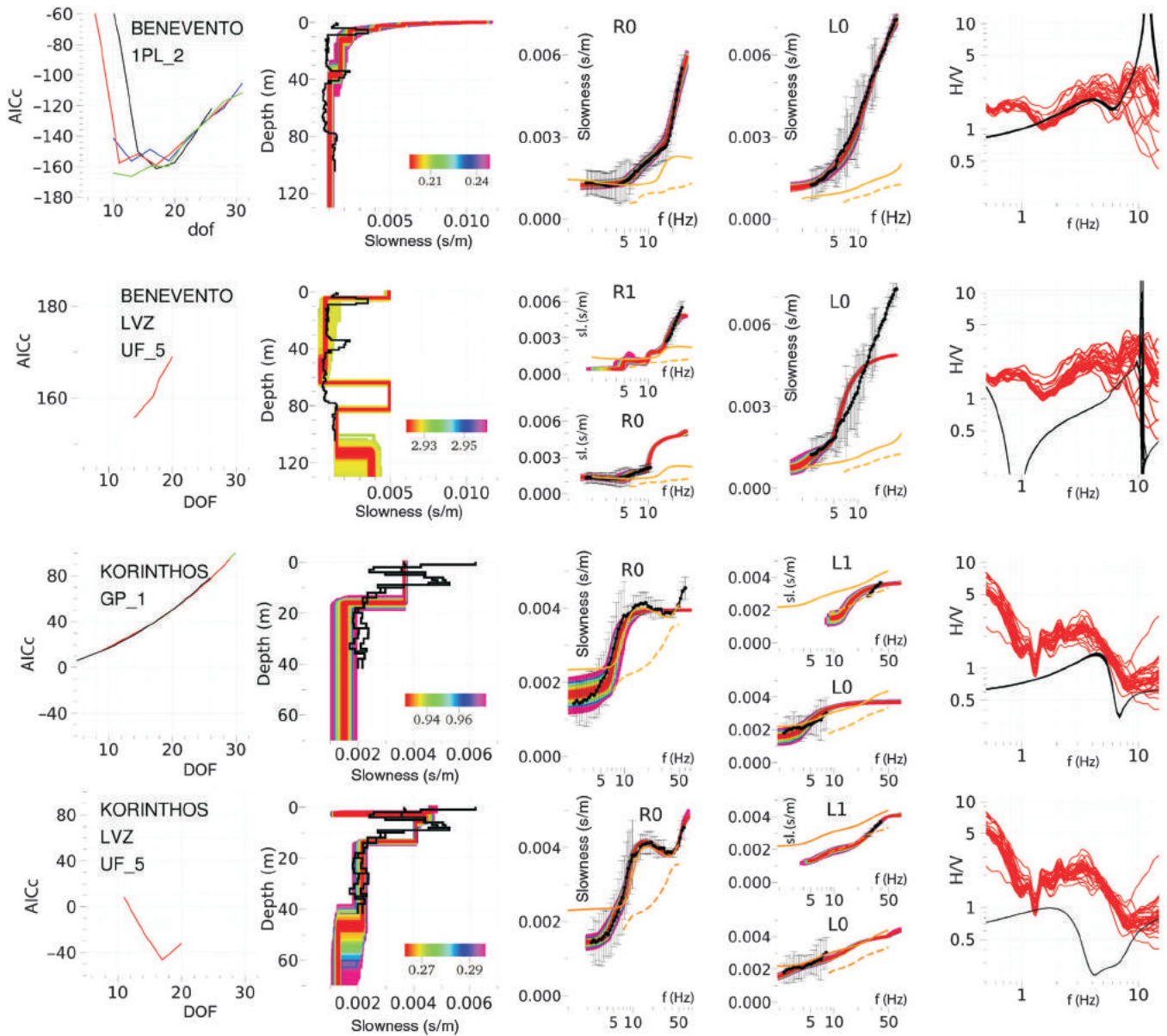


Figure 9. Results at Benevento and Korinthos. At both sites, the inversions have been performed with (second and fourth row) and without (first and third row) LVZ. Graphical schemes for AICc, slowness profiles, and dispersion curves are described in the caption of Figure 3. The H/V curves are as described in the caption of Figure 4.

Rayleigh and Love wave dispersion curves to improve the accuracy of the estimated  $V_S$  profiles in presence of an LVZ.

At Benevento, the inversion without LVZ (Figure 9, first row) leads to a good match between observed and inverted dispersion curves (misfit  $< 0.25$ ). The theoretical ellipticities also agree well with the H/V spectral ratios at frequencies above 1 Hz (Figure 9, first row). The  $V_S$  profile provided by a crosshole survey (Di Giulio et al., 2008) is not matched by the inverted models. The discrepancy in  $V_{S30}$  ( $\Delta V_{S30}$  of 48%, see Table 1) between the reference crosshole model and inverted models is very high (740 versus 383 m/s, respectively). To account the velocity reversal shown by crosshole data, we repeat the inversion allowing LVZ. We use a parameterization of the model space assuming uniform layers over a half-space, as indicated by the crosshole profile. All the inversions performed for Benevento, including fundamental modes and LVZ, produce unsatisfactory results with a very high misfit; we therefore perform the inversion considering different modes interpretation. Figure 9 (second row) shows one modeling example where the experimental dispersion curves are assumed to be fundamental Rayleigh mode (R0), first higher Rayleigh mode (R1) and fundamental Love mode (L0). Although in this case, the disagreement in  $V_{S30}$  decreases (from 740 to 710 m/s for this inversion, see Table 1), the inversion including LVZ still returns a  $V_S$  profile very different from the crosshole survey and the theoretical ellipticities do not match the observed H/V curves (Figure 9, second row). Failure of our inversion considering LVZ is also evidenced by the mismatch on the Love wave fundamental mode above 12 Hz, and this causes a very large misfit (about 2.9). Our inversion strategy at Benevento after the inclusion of LVZ clearly fails related to the complexity of the layered structure. A forward computation of the fundamental Rayleigh and Love mode, using an initial  $V_S$  model constrained by the crosshole profile, is able to provide theoretical dispersion curves that reasonably agree with the experimental curves (not shown).

At Korinthos, the inversion without LVZ (Figure 9, third row) shows a large misfit (about 0.9), and the increase in DOF (Figure 9, third row) does not contribute to decrease the AICc. The lowest AICc is yielded by the simplest model parameterization (i.e., one layer over the half-space; see Table 2), but the inverted models do not match the borehole data indicating some problems in the surface-wave inversion of this site. The available downhole and crosshole data present evidence of a more complex layering than a simple soft layer over the half-space. The shape of the experimental Rayleigh wave dispersion curve suggests a possible effect of LVZ between 20 and 40 Hz (Figure 9). We repeat the inversion using a model parameterization with uniform layering allowing LVZ (Figure 9, fourth row). We vary the number of uniform layers in the UF parameterization (from UF\_3 to UF\_6 of Table 2) allowing LVZ in the third  $V_S$  layer, as indicated by borehole profile. We tested that an inversion with the possibility of LVZ within each layer, although this significantly increases the CPU resource, do not improve the final inverted models of this site. The best parameterization of Korinthos, including LVZ, is clearly indicated by the AICc evolution versus DOF, with a minimum DOF corresponding to five uniform layers (Figure 9, fourth row). The results show a nice match of the experimental dispersion curves with the theoretical curve (misfit about 0.27). The shear-wave slowness profiles resulting from the inversion indicate a thin LVZ in fairly good agreement with the borehole

profiles, although the H/V ratios are still not fit by the theoretical ellipticities.

Thus, we find contrasting results at the two investigated sites: (1) Our inversion strategy fails at Benevento, where we cannot reproduce the borehole velocity profile by modeling with or without a LVZ. It is the inversion without considering a LVZ that returns a better fit in terms of dispersion and H/V curves (Figure 9, first row). (2) On the other hand, at Korinthos, the borehole profile has been well-reproduced, and the fit to the measured dispersion curves has improved by including LVZ during the inversion (Figure 9, fourth row).

## DISCUSSION

The inversion of dispersion curves is a nonunique problem and is probably the most difficult step in surface-wave methods aimed at deriving the shear-wave-velocity profile. We propose a strategy through which different parameterizations of the model space can be extensively explored and ranked during the inversion analysis. The goal is quantitative evaluation among reliable model parameterizations that explain satisfactorily the experimental data rather than precise estimation of a single  $V_S$  profile at a specific site. The final result is not a single optimum model, rather a best set of models derived from the same parameterization class. We invert surface-wave dispersion curves at different European strong-motion sites (in terms of urban/rural environment, stiff/soft sites, shallow/deep bedrock interface), where dispersion curves have been estimated in a broad frequency band (with the wavelengths ranging from 1 m to hundreds of meters; see Table 1). We do not consider independent constraints within the inversion process to test our inversion strategy that is first based on a multimodel parameterization and then on an information criterion.

In detail, we adopt four distinct classes of parameterization commonly used for the model space. Of course, the classes of parameterization can be modified or increased in the case of independent information on the geotechnical structure. We evaluate in a quantitative way the best parameterization of the model space according to Akaike's information approach. AICc represents a theoretical compromise between the maximum log likelihood and the number of free parameters and is an effective tool for ranking equivalent models in terms of misfit.

The approach of this paper can be regarded as an improvement of the first step of the inversion strategy proposed by Renalier et al. (2010), in which they suggest a two-step inversion procedure at sites with strong impedance contrast for orienting the inversion search within the parameter space. The first step estimated a bedrock depth range using the evolution of the minimum misfit and of the corresponding bedrock depth versus the number of homogeneous layers (the UF class of this paper). The second step was a constrained inversion assuming a linear velocity law (1L class) and using the bedrock depth range provided by the inversion within the first step. Renalier et al. (2010) considered a single given parameterization (UF) for investigating the influence of model parameterization, and the selection of the optimum model is based exclusively on the misfit function (equation 1) and on its evolution with number of layers (see Figure 2c). In this study, we investigate four classes of parameterization searching for the most suitable parameterization (if any) in the inversion process. We compare the performance of the four classes in a quantitative

way by combining the misfit to the Akaike's information criterion. We prefer not to introduce any information from independent measurements during the inversion. Of course, additional constraints provided from independent data or extracted from the inversion process itself (following the second step of Renalier et al., 2010) can direct the inversion to more reliable results. Assuming the H/V noise spectral ratios and the  $V_S$  profiles from borehole data are a priori and independent information, we generally find a good agreement between the velocity structure derived from inversion and the independent information. The  $V_S$  profiles derived from inversion are generally reliable for analysis of ground-motion estimation. We also find a satisfactory agreement in the  $V_{S30}$  estimates, with the error ( $\Delta V_{S30}$ ) increasing for stiffer sites ( $V_{S30} > 650$  m/s) and lower than 20% on average (Figure 10). The largest discrepancies in the near-surface  $V_S$  profiles are observed at the sites of Norcia and Benevento ( $V_{S30}$  of 35% and of 48% not allowing LVZ); the inversion procedure reproduces the observed dispersion curves but not the borehole profiles (see Figures 3 and 9) suggesting some failure in the initial assumptions or an inability of the inversion to match high-contrast LVZs. Both Norcia and Benevento are stiff and deep sites (bedrock depth more than 100 m) with a complex soil structure including thick LVZs as shown by the reference borehole profiles. In principle, the presence of LVZ could be included in our strategy through ad hoc model parameterization, but this presently has some practical limitation. The presence of LVZ increases drastically the nonuniqueness of the problem, the number of DOF describing the problem, and consequently, the efficiency and time computation of the most popular inversion algorithm. However, the computational time with today's infrastructure is not considered a drawback (Cadet and Savvaidis, 2011).

The best parameterizations of the model space according to the Akaike criterion mostly consist in three or four layers over a half-space (Figure 11). These layers follow a uniform or a power-law velocity-depth function over a half-space (Figure 11), corresponding to a number of DOF between 11 and 14 (see Table 2). This result is valid for the sites of Table 1; studies involving both a larger database and different constraints on the surface-wave inversion are needed to confirm the existence of an optimal class

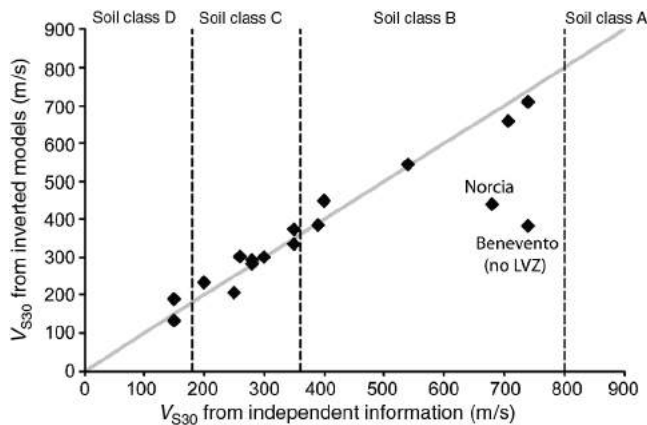


Figure 10. Comparison between  $V_{S30}$  from independent a priori information and  $V_{S30}$  derived from inversion. The main outliers from the gray unity line are observed at the Norcia and Benevento sites (see Table 1).

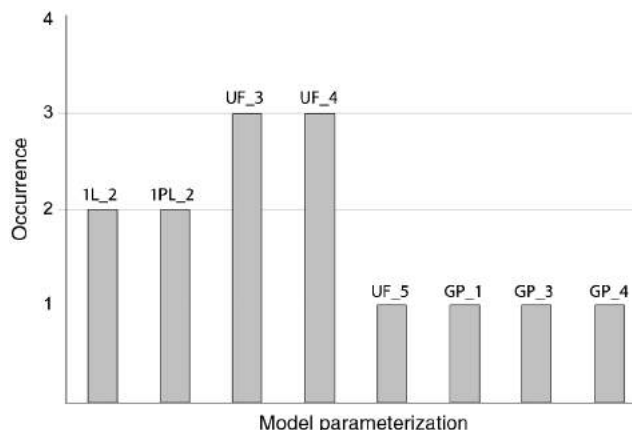


Figure 11. The histogram shows the distribution of the best model classes (lowest AICc number) for the NERIES sites of Table 1. On the x-axis the best model parameterization (Table 2), on the y-axis the number of occurrences. UF, 1PL, 1L, and GP indicate the four parameterization groups described in the text. The last number in the names of model parameterizations indicates the number of uniform layers over the half-space.

of models in the inversion analysis. The description of the best set of models found from our inversion strategy is given in Appendix A, including also the compressional velocity. The highest  $V_P/V_S$  ratios found for few sites (e.g., Buia in Appendix A), which correspond to the maximum  $V_P$  and Poisson's ratio allowed within the inversion (5000 m/s and 0.5, respectively), are questionable for the uppermost layers indicating a possible overestimation of the real  $V_P$  values.

## CONCLUSIONS

In this paper, we examined general resolution issues, the lateral heterogeneity of the subsoil, low-velocity layers, and misinterpretation of modes that are all potential sources of bias in the inversion analysis. The inversion strategy based on AICc is not able to resolve the general problems of the surface-wave analysis, and with wrong initial assumptions, increasing the complexity of the model is not useful. Large misfit and an unclear minimum of AICc when varying the DOF can only suggest a failure of the inversion. Conversely, the proposed strategy is effective in selecting a class of models parameterization according to a well-known and objective criterion of selection. Models with similar misfits are ranked by penalizing the model complexity. Our strategy can be viewed as somewhat automated and can be applied to many sites for investigating and ranking a large number of models. The modern computers can easily supply the computational time and amount of data storage required by our inversion strategy. This strategy has been tested with success on 14 strong-motion sites where specific near-surface characterizations are available. A "standard" inversion, dealing with a limited number of model parameters, could also provide better results at a single site, although both the selection of the starting model parameterization and of the optimum final model usually depends on the interpreter's choice.

Regarding the applicability of the neighborhood algorithm in conjunction with AICc, even if different inversion algorithms can be used in surface-wave inversion, we use the neighborhood

algorithm because of its feasibility and performance. The improved neighborhood algorithm finalizes the search into the most promising parameter space with a good ability to escape from local minimums. It is based on inequality constraints because the search intervals for the free parameters are not necessarily equal. The two classes of parameterization, UF and GP, are defined by the same number of DOF, although they differ in the search interval of the free parameter thickness. The model parameterization with and without prohibition of LVZ also introduces inequality constraints because the search intervals of free parameters are different in the two cases. From a statistical point of view, the Akaike information criterion is one among others that may be used to correct for the model complexity. It should be noted that any implementation of an information criterion can be included in the proposed inversion approach for exploring the influence of parameterization and for ranking the most representative models.

### ACKNOWLEDGMENTS

This research was financially supported by both the ITSAK-GR EC-Project (International Transfer of Seismological Advanced Knowledge and Geophysical Research, a Transfer of Knowledge Marie-Curie action; MTKD-CT-2005-0296270), and the NERIES EC-Project (Network of Research Infrastructures for European Seismology, # RII3-CT-2006-026130; JRA4). Special thanks to Heloise Cadet, Maria Daphne Mangriotis, and Elena Zargli for their support and constructive comments. Preliminary results of this work were shown at the 14th ECEE meeting (Ohrid-FYROM, 2010, abstract number 1434). The authors wish to thank the associate editor Michael Asten, Maxime Claproud, William Stephenson, and two anonymous reviewers for many valuable remarks that helped in improving the manuscript.

### APPENDIX A

#### BEST-FIT MODELS

The best-fit models derived from our inversion strategy are listed in Table A-1 for all the sites of Table 1, except for Benevento, where we cannot find a consistent solution with the borehole reference data (Figure 9). The best-fit model is assumed as the lowest misfit model into the parameterization class selected by the AICc approach (Figures 3, 5, 7, 8, and 9; first column).

In Table A-1, the first three lines of the tabulated models are header rows indicating: (1) the site; (2) the parameterization class where the minimum AICc is found; (3) the index of the model at lowest misfit and the corresponding misfit value. The first row without “#” indicates the total number of layers (including half-space). The values of thickness (m),  $V_P$  (m/s), and  $V_S$  (m/s) are then listed in three columns (the last row with thickness 0 refers to half-space). Density of each layer was fixed to 2 g/cm<sup>3</sup> during the inversion.

The uncertainties, in terms of minimum and maximum  $V_S$  profiles derived from our inversion strategy, are shown in the last table (Table A-2) of this Appendix for the first 100 m. The minimum and maximum  $V_S$  profiles of Table A-2 correspond to the upper and lower boundary of the slowness/depth plots into Figures 3, 5, 7, 8, and 9 (second column).

**Table A-1 Best model derived from the inversion using the AICc approach for each site. Further description is given in the text.**

<hr/>				
# Aigio				
# 1L_2				
# Layered	Model	181,802:		m = 0.2922
8				
0.52	345	211		
0.52	423	259		
0.52	500	306		
0.52	578	354		
0.52	655	401		
6.7	701	429		
21	2336	678		
0	2359	1407		
# Bolu				
# 1PL_2				
# Layered	Model	77,678:		m = 0.2584
8				
0.08	205	84		
0.17	207	89		
0.34	212	98		
0.68	219	114		
1.4	229	140		
21	908	297		
60	4926	474		
0	4975	831		
# Buia				
# 1L_2				
# Layered	Model	65,800:		m = 0.2182
8				
0.32	4786	61		
0.32	4796	75		
0.32	4805	89		
0.32	4815	103		
0.32	4824	117		
4.1	4877	192		
28	4926	412		
0	4975	864		
# Colf_loc1				
# GP_1				
# Layered	Model	2744:		m = 0.3054
2				
44	397	190		
0	4975	3028		
# Colf_loc2				
# UF_4				
# Layered	Model	114,830:		m = 0.2670
5				

**Table A-1 Best model derived from the inversion using the AICc approach for each site. Further description is given in the text. (Continued)**

1.2	202	50.5	
5	204	98	
9	4877	131	
52	4926	179	
0	4975	537	
# Düzce			
# UF_3			
# Layered	Model	19,350:	m = 0.3246
4			
3.5	289	177	
11	4877	229	
52	4926	455	
0	4975	610	
# Forlì			
# GP_4			
# Layered	Model	43,522:	m = 0.2514
5			
0.1	202	124	
6.5	422	258	
29.5	552	338	
137	1211	741	
0	4975	3028	
# Knidi			
# GP_3			
# Layered	Model	10,242:	m = 1.1654
4			
0.8	329	201	
14	694	425	
182	4926	1870	
0	4975	3028	
# Korinthos_LVZ			
# UF_5			
# Layered	Model	179,232:	m = 0.2668
6			
2.1	382	216	
1.2	1649	852	
2.6	1665	227	
7.6	4877	246	
33	4926	460	
0	4975	767	
# Nestos			
# UF_3			
# Layered	Model	17,241:	m = 0.3129
4			
2.9	244	149	
21.3	1260	199	
25.4	2658	312	

**Table A-1 Best model derived from the inversion using the AICc approach for each site. Further description is given in the text. (Continued)**

0	2685	1634	
# Norcia			
# UF_4			
# Layered	Model	136,402:	m = 0.3544
5			
1.4	202	103	
4.7	1064	266	
6.6	1075	438	
121	1733	795	
0	2907	1769	
# Sakarya			
# UF_4			
# Layered	Model	137,452:	m = 0.3274
5			
1.4	1023	83	
3.2	1600	243	
7.4	1616	400	
158	1632	999	
0	2406	1464	
# Sturno			
# 1PL_2			
# Layered	Model	190,795:	m = 0.1614
8			
0.05	203	65	
0.1	207	70	
0.2	213	81	
0.4	224	103	
0.8	242	148	
15	4877	359	
52	4926	608	
0	4975	822	
# Volvi			
# UF_3			
# Layered	Model	33,350:	m = 0.3456
4			
4.7	281	172	
15.2	4877	205	
113	4926	400	
0	4975	1916	



Table A-2. Description of the minimum and maximum  $V_S$  profiles derived from the inversion (first 100 m).

Depth (m)	Aigio		Bolu		Buia		Colf loc1		Colf loc2		Düzce		Forlì	
	$V_{S\_min}$ (m/s)	$V_{S\_max}$ (m/s)	$V_{S\_min}$ (m/s)	$V_{S\_max}$ (m/s)	$V_{S\_min}$ (m/s)	$V_{S\_max}$ (m/s)	$V_{S\_min}$ (m/s)	$V_{S\_max}$ (m/s)	$V_{S\_min}$ (m/s)	$V_{S\_max}$ (m/s)	$V_{S\_min}$ (m/s)	$V_{S\_max}$ (m/s)	$V_{S\_min}$ (m/s)	$V_{S\_max}$ (m/s)
0	186	223	80	90	60	63	184	195	51	70	173	179	72	130
1	252	306	112	117	91	108	184	195	51	70	173	179	121	261
2	343	420	131	149	186	201	184	195	98	110	173	179	231	261
3	416	438	291	309	186	201	184	195	98	110	173	225	231	261
4	416	438	291	309	186	201	184	195	98	110	218	236	231	261
5	416	438	291	309	186	201	184	195	98	110	218	236	234	325
10	420	741	291	309	388	455	184	195	127	146	218	236	321	341
15	639	756	291	309	388	455	184	195	127	180	222	503	321	341
20	639	756	291	503	388	455	184	195	138	197	274	547	321	341
25	639	756	291	545	388	455	184	195	173	199	315	563	321	341
30	651	1634	297	550	388	455	184	195	173	199	334	575	321	341
35	685	2180	412	550	392	964	184	195	173	199	366	592	321	749
40	1142	2457	412	550	416	1044	184	490	173	199	373	598	338	923
50	1142	2457	412	550	455	1188	186	3028	173	199	400	629	651	923
60	1142	2457	429	759	798	1188	286	3028	173	199	416	641	651	923
70	1142	2457	438	839	798	1188	286	3028	175	2910	433	681	651	923
80	1142	2457	438	927	798	1188	286	3028	186	3028	446	694	651	923
90	1142	2457	455	1034	798	1188	286	3028	382	3028	451	775	651	923
100	1142	2457	474	1055	798	1188	286	3028	382	3028	451	908	651	923

Depth (m)	Korinthos_lvz		Nestos		Norcia		Sakarya		Sturno		Volvi	
	$V_{S\_min}$ (m/s)	$V_{S\_max}$ (m/s)	$V_{S\_min}$ (m/s)	$V_{S\_max}$ (m/s)	$V_{S\_min}$ (m/s)	$V_{S\_max}$ (m/s)	$V_{S\_min}$ (m/s)	$V_{S\_max}$ (m/s)	$V_{S\_min}$ (m/s)	$V_{S\_max}$ (m/s)	$V_{S\_min}$ (m/s)	$V_{S\_max}$ (m/s)
0	212	218	146	152	100	109	80	86	54	81	168	177
1	212	218	146	152	100	109	80	86	120	200	168	177
2	212	218	146	152	241	288	238	248	306	381	168	177
3	756	941	148	203	241	288	238	248	306	381	168	177
4	212	241	193	205	241	288	238	248	306	381	168	177
5	214	246	193	205	241	416	246	442	306	381	170	214
10	243	248	193	205	377	493	373	442	318	508	195	227
15	433	539	193	205	741	844	923	1040	338	620	195	227
20	433	539	193	269	741	844	923	1040	438	658	199	425
25	433	539	195	381	741	844	923	1040	438	658	381	438
30	433	539	199	608	741	844	923	1040	438	759	381	438
35	433	539	234	905	741	844	923	1040	469	782	381	438
40	433	775	246	1823	741	844	923	1040	488	790	381	438
50	442	856	277	2852	741	844	923	1040	529	847	381	438
60	469	917	362	2852	741	844	923	1040	556	856	381	438
70	513	917	429	2852	741	844	923	1040	578	945	381	438
80	694	917	523	2852	741	844	923	1040	596	945	381	438
90	694	917	608	2852	741	1076	923	1040	614	945	381	438
100	694	917	715	2852	741	1602	923	1040	614	945	381	438

## REFERENCES

- Akaike, H., 1973, Information theory as an extension of the maximum likelihood principle: 2nd International Symposium on Information Theory, eds., B. N. Petrov, and F. Csaki, 267–281.
- Akaike, H., 1974, A new look at the statistical model identification: IEEE Transactions on Automatic Control, **19**, no. 6, 716–723.
- Akaike, H., 1980, Likelihood and the Bayes procedure: Trabajos de Estadística y de Investigación Operativa, **31**, 143–166, doi: [10.1007/BF02888350](https://doi.org/10.1007/BF02888350).
- Aki, K., 1957, Space and time spectra of stationary stochastic waves, with special reference to microtremors: Bulletin of the Earthquake Research Institute of Tokyo University, **25**, 415–457.
- Anraku, K., 1999, An information criterion for parameters under a simple order restriction: Biometrika, **86**, 141–152, doi: [10.1093/biomet/86.1.141](https://doi.org/10.1093/biomet/86.1.141).
- Aoudia, A., A. Saraó, B. Bukchin, and P. Suhadolc, 2000, The 1976 Friuli (NE Italy) thrust faulting earthquake: A reappraisal 23 years later: Geophysical Research Letters, **27**, 573–576, doi: [10.1029/1999GL011071](https://doi.org/10.1029/1999GL011071).
- Arai, H., and K. Tokimatsu, 2004, S-wave velocity profiling by inversion of microtremor H/V spectrum: Bulletin of the Seismological Society of America, **94**, 53–63, doi: [10.1785/0120030028](https://doi.org/10.1785/0120030028).
- Arai, H., and K. Tokimatsu, 2005, S-wave velocity profiling by joint inversion of microtremor dispersion curve and horizontal-to-vertical (H/V) spectrum: Bulletin of the Seismological Society of America, **95**, 1766–1778, doi: [10.1785/0120040243](https://doi.org/10.1785/0120040243).
- Asten, M. W., 2006a, On bias and noise in passive seismic data from finite circular array data processed using SPAC methods: Geophysics, **71**, no. 6, V153–V162, doi: [10.1190/1.2345054](https://doi.org/10.1190/1.2345054).
- Asten, M. W., 2006b, Site shear velocity profile interpretation from microtremor array data by direct fitting of spac curves, in P. Y. Bard, E. Chaljub, C. Cornou, F. Cotton, and P. Guéguen, eds., Proceedings of the 3rd International Symposium on the Effects of Surface Geology on Seismic Motion (ESG2006), **2**, LCPC, 1069–1082; [www.geosci.monash.edu.au/research/cegas](http://www.geosci.monash.edu.au/research/cegas).
- Asten, M. W., and D. M. Boore, 2005, Comparison of shear-velocity profiles of unconsolidated sediments near the Coyote borehole (CCOC) measured with fourteen invasive and non-invasive methods, in M. W. Asten, and D. M. Boore, eds., Blind comparisons of shear-wave velocities at closely spaced sites in San Jose, California: U.S. Geological Survey Open-File Report, 2005–1169; <http://pubs.usgs.gov/of/2005/1169/>.
- Asten, M. W., N. Lam, G. Gibson, and J. Wilson, 2002, Microtremor survey design optimized for application to site amplification and resonance modelling, in M. Griffith, D. Love, P. McBean, A. McDougall, and B. Butler, eds., Total risk management in the privatized era: Proceedings of the Australian Earthquake Engineering Society, Paper 7.
- Bard, P. Y., H. Cadet, B. Endrun, M. Hobiger, F. Renalier, M. Theodulidis, D. Ohrnberger, F. Fäh, F. Sabetta, and P. Teves-Costa, 2010, From non-invasive site characterization to site amplification: Recent advances in the use of ambient vibration measurements: Earthquake Engineering in Europe, **17**, Part 2, 105–123, doi: [10.1007/978-90-481-9544-2\\_5](https://doi.org/10.1007/978-90-481-9544-2_5).
- Bard, P. Y., and M. Bouchon, 1985, The two-dimensional resonance of sediment-filled valleys: Bulletin of the Seismological Society of America, **75**, 519–541.
- Beauval, C., P. Y. Bard, P. Moczo, and J. Kristek, 2003, Quantification of frequency-dependent lengthening of seismic ground-motion duration due to local geology: Applications to the Volvi area (Greece): Bulletin of the Seismological Society of America, **93**, 371–385, doi: [10.1785/0120010255](https://doi.org/10.1785/0120010255).
- Bettig, B., P. Y. Bard, F. Scherbaum, J. Riepl, F. Cotton, C. Cornou, and D. Hatzfeld, 2001, Analysis of dense array noise measurements using the modified spatial auto-correlation method (SPAC). Application to the Grenoble area: Bollettino di Geofisica Teorica e Applicata, **42**, 281–304.
- Bonnefoy-Claudet, S., C. Cornou, P. Y. Bard, F. Cotton, P. Moczo, J. Kristek, and D. Fäh, 2006, H/V ratio: A tool for site effects evaluation. Results from 1D noise simulations: Geophysical Journal International, **167**, 827–837, doi: [10.1111/gji.2006.167.issue-2](https://doi.org/10.1111/gji.2006.167.issue-2).
- Boore, D. M., and M. W. Asten, 2008, Comparisons of shear-wave slowness in the Santa Clara Valley, California, using blind interpretations of data from invasive and non-invasive methods: Bulletin of the Seismological Society of America, **98**, 1983–2003, doi: [10.1785/0120070277](https://doi.org/10.1785/0120070277).
- Boore, D. M., and E. M. Thompson, 2007, On using surface-source down-hole-receiver logging to determine seismic slownesses: Soil Dynamics and Earthquake Engineering, **27**, 971–985, doi: [10.1016/j.soildyn.2007.03.005](https://doi.org/10.1016/j.soildyn.2007.03.005).
- Boore, D. M., E. M. Thompson, and H. Cadet, 2011, Regional correlations of  $V_{S30}$  and velocities averaged over depths less than and greater than 30 m: Bulletin of the Seismological Society of America, **101**, 3046–3059, doi: [10.1785/0120110071](https://doi.org/10.1785/0120110071).
- Bozdogan, H., 2000, Akaike's information criterion and recent developments in information complexity: Journal of Mathematical Psychology, **44**, 62–91, doi: [10.1006/jmps.1999.1277](https://doi.org/10.1006/jmps.1999.1277).
- Brown, L. T., D. M. Boore, and K. H. Stokoe II, 2002, Comparison of shear-wave slowness profiles at 10 strong-motion sites from non invasive SASW measurements and measurements made in boreholes: Bulletin of the Seismological Society of America, **92**, 3116–3133, doi: [10.1785/0120020030](https://doi.org/10.1785/0120020030).
- Burnham, K. P., and D. R. Anderson, 2001, Kullback-Leibler information as a basis for strong inference in ecological studies: Wildlife Research, **28**, 111–119, doi: [10.1071/WR99107](https://doi.org/10.1071/WR99107).
- Burnham, K. P., and D. R. Anderson, 2004, Multimodel inference understanding AIC and BIC in model selection: Sociological Methods Research, **33**, no. 2, 261–304, doi: [10.1177/0049124104268644](https://doi.org/10.1177/0049124104268644).
- Cadet, H., and A. Savvaidis, 2011, Comparative application of dispersion curve inversion strategies. Case study of noise arrays in the Euroseistest site, Greece: Near Surface Geophysics, **9**, 571–583, doi: [10.3997/1873-0604.2011043](https://doi.org/10.3997/1873-0604.2011043).
- Capon, J., 1969, High-resolution frequency-wavenumber spectrum analysis: Proceeding of the IEEE, **57**, no. 8, 1408–1418, doi: [10.1109/PROC.1969.7278](https://doi.org/10.1109/PROC.1969.7278).
- Cara, F., G. Di Giulio, G. Milana, P. Bordoni, J. Haines, and A. Rovelli, 2010, On the stability and reproducibility of the horizontal-to-vertical spectral ratios on ambient noise: Case study of Cavola, northern Italy: Bulletin of the Seismological Society of America, **100**, 1263–1275, doi: [10.1785/0120090086](https://doi.org/10.1785/0120090086).
- Castellaro, S., and F. Mulargia, 2009,  $V_{S30}$  estimates using constrained H/V measurements: Bulletin of the Seismological Society of America, **99**, 761–773, doi: [10.1785/0120080179](https://doi.org/10.1785/0120080179).
- CEN (COMITÉ EUROPÉEN DE NORMALISATION), 2004, EN 1998-1 Eurocode 8: design of structures for earthquake resistance. Part 1: General rules, seismic actions and rules for buildings.
- Cercato, M., F. Cara, E. Cardarelli, G. Di Giulio, G. Di Filippo, and G. Milana, 2010, Shear-wave velocity profiling at sites with high stiffness contrasts: A comparison between invasive and non-invasive methods: Near Surface Geophysics, **8**, 75–94, doi: [10.3997/1873-0604.2009053](https://doi.org/10.3997/1873-0604.2009053).
- Chaljub, E. O., P. Y. Bard, S. Tsuno, J. Kristek, P. Moczo, P. Franek, F. Hollender, M. Manakou, D. Raptakis, and K. Ptilakis, 2009, Assessing the capability of numerical methods to predict earthquake ground motion: The Euroseistest verification and validation project: American Geophysical Union, Abstract #S43A-1968.
- Cho, I., T. Tada, and Y. Shinozaki, 2004, A new method to determine phase velocities of Rayleigh waves from microseisms: Geophysics, **69**, 1535–1551, doi: [10.1190/1.1836827](https://doi.org/10.1190/1.1836827).
- Cho, I., T. Tada, and Y. Shinozaki, 2006, A generic formulation for microtremor exploration methods using three-component records from a circular array: Geophysical Journal International, **165**, 236–258, doi: [10.1111/gji.2006.165.issue-1](https://doi.org/10.1111/gji.2006.165.issue-1).
- Chouet, B. A., P. B. Dawson, G. De Luca, M. Martini, G. Milana, G. Saccorotti, and R. Scarpa, 1998, Array analyses of seismic sources at Stromboli Volcano: Acta Vulcanologica, **10**, 2, 367–382.
- Claprod, M., and M. W. Asten, 2009, Initial results from spatially averages coherency, frequency-wavenumber, and horizontal to vertical spectrum ratio microtremor surveys for site hazard study at Launceston, Tasmania: Exploration Geophysics, **40**, 132–142, doi: [10.1071/EG08106](https://doi.org/10.1071/EG08106).
- Claprod, M., M. W. Asten, and J. Kristek, 2011, Using the SPAC microtremor method to identify 2D effects and evaluate 1D shear-wave velocity profile in valleys: Bulletin of the Seismological Society of America, **101**, 826–847, doi: [10.1785/0120090232](https://doi.org/10.1785/0120090232).
- Cornou, C., M. Ohrnberger, D. M. Boore, K. Kudo, and P. Y. Bard, 2006, Derivation of structural models from ambient vibration array recordings: Results from an international blind test, in P. Y. Bard, E. Chaljub, C. Cornou, F. Cotton, and P. Guéguen, eds., Proceedings of the 3rd International Symposium on the Effects of Surface Geology on Seismic Motion (ESG2006), **2**, 1127–1219.
- Di Giulio, G., C. Cornou, M. Ohrnberger, M. Wathelet, and A. Rovelli, 2006, Deriving wavefield characteristics and shear-velocity profiles from two-dimensional small-aperture arrays analysis of ambient vibrations in a small-size alluvial basin Colfiorito, Italy: Bulletin of the Seismological Society of America, **96**, 1915–1933, doi: [10.1785/0120060119](https://doi.org/10.1785/0120060119).
- Di Giulio, G., L. Improta, G. Calderoni, and A. Rovelli, 2008, A study of the seismic response of the city of Benevento (southern Italy) through a combined analysis of seismological and geological data: Engineering Geology, **97**, 146–170, doi: [10.1016/j.enggeo.2007.12.010](https://doi.org/10.1016/j.enggeo.2007.12.010).
- Di Giulio, G., A. Rovelli, F. Cara, R. M. Azzara, F. Marra, R. Basili, and A. Caserta, 2003, Long-duration asynchronous ground motions in the Colfiorito plain, central Italy, observed on a two-dimensional dense array: Journal of Geophysical Research, **108**, 2486, doi: [10.1029/2002JB002367](https://doi.org/10.1029/2002JB002367).
- Dunkin, J. W., 1965, Computation of modal solutions in layered elastic media at high frequencies: Bulletin of the Seismological Society of America, **55**, 335–358.
- Endrun, B., M. Ohrnberger, and A. Savvaidis, 2010, On the repeatability and consistency of three-component ambient vibration array measurements:

- Bulletin of Earthquake Engineering, **8**, 535–570, doi: [10.1007/s10518-009-9159-9](https://doi.org/10.1007/s10518-009-9159-9).
- Endrun, B., and F. Renalier, 2008, Report on in-situ measurements at the 20 selected sites, NERIES project JRA4 task C, EU-FP6 EC: Project number 026130, deliverable D2, <http://www.neries-eu.org/?subpage=/projectweb/portalproject/Deliverables.html>, accessed 28 December 2011.
- Fäh, D., F. Kind, and D. Giardini, 2001, A theoretical investigation of average H/V ratios: *Geophysical Journal International*, **145**, 535–549, doi: [10.1046/j.0956-540x.2001.01406.x](https://doi.org/10.1046/j.0956-540x.2001.01406.x).
- Fäh, D., P. Suhadolc, and G. F. Panza, 1993, Variability of seismic ground motion in complex media: The case of a sedimentary basin in the Friuli (Italy) area: *Journal of Applied Geophysics*, **30**, no. 1–2, 131–148, doi: [10.1016/0926-9851\(93\)90022-Q](https://doi.org/10.1016/0926-9851(93)90022-Q).
- Fäh, D., M. Wathelet, M. Kristekova, H. Havenith, B. Endrun, G. Stamm, V. Poggi, J. Burjanek, and C. Cornou, 2009, Report on software on inversion of H/V ellipticity, NERIES project JRA4 task B2, EU-FP6 EC: Project number 026130, deliverable D4, <http://www.neries-eu.org/?subpage=/projectweb/portalproject/Deliverables.html>, accessed 28 December 2011: Technical report.
- Foti, S., C. Comina, D. Boiero, and L. V. Socco, 2009, Non uniqueness in surface wave inversion and consequences on seismic site response analyses: *Soil Dynamics and Earthquake Engineering*, **29**, no. 6, 982–993, doi: [10.1016/j.soildyn.2008.11.004](https://doi.org/10.1016/j.soildyn.2008.11.004).
- Foti, S., S. Parolai, P. Bergamo, G. Di Giulio, M. Maraschini, G. Milana, M. Picozzi, and R. Puglia, 2011, Surface wave surveys for seismic site characterization of accelerometric stations in ITACA: *Bulletin of Earthquake Engineering*, doi: [10.1007/s10518-011-9306-y](https://doi.org/10.1007/s10518-011-9306-y).
- García-Jerez, A., F. Luzón, and M. Navarro, 2008, An alternative method for calculation of Rayleigh and Love wave phase velocities by using three-component records on a single circular array without a central station: *Geophysical Journal International*, **173**, 844–858, doi: [10.1111/gji.2008.173.issue-3](https://doi.org/10.1111/gji.2008.173.issue-3).
- Haghshenas, E., P. Y. Bard, and N. Theodoulidis, 2008, Empirical evaluation of microtremor H/V spectral ratio: *Bulletin of Earthquake Engineering*, **6**, 75–108, doi: [10.1007/s10518-007-9058-x](https://doi.org/10.1007/s10518-007-9058-x).
- Hamimu, L., J. Safani, and M. Nawawi, 2011, Improving the accurate assessment of a shear-wave velocity reversal profile using joint inversion of the effective Rayleigh wave and multimode Love wave dispersion curves: *Near Surface Geophysics*, **9**, 1–14, doi: [10.3997/1873-0604.2010029](https://doi.org/10.3997/1873-0604.2010029).
- Herrmann, R. B., 1987, Computer programs in seismology, **IV**: St. Louis University.
- Hobiger, M., P. Y. Bard, C. Cornou, and N. Le Bihan, 2009, Single station determination of Rayleigh wave ellipticity by using the random decrement technique (RayDec): *Geophysical Research Letters*, **36**, L14303, doi: [10.1029/2009GL038863](https://doi.org/10.1029/2009GL038863).
- Hurvich, C. M., and C. L. Tsai, 1989, Regression and time series model selection in small samples: *Biometrika*, **76**, 297–307, doi: [10.1093/biomet/76.2.297](https://doi.org/10.1093/biomet/76.2.297).
- Ibs-von Seht, M., and W. Jürgen, 1999, Wohlenberg microtremor measurements used to map thickness of soft sediments: *Bulletin of the Seismological Society of America*, **89**, 250–259.
- Jongmans, D., K. Ptilakis, D. Demanet, D. Raptakis, J. Riepl, C. Horrent, G. Tsokas, K. Lontzetidis, and P. Y. Bard, 1998, Euroseistest: Determination of the geological structure of the Volvi basin and validation of the basin response: *Bulletin of the Seismological Society of America*, **88**, 473–487.
- Köhler, A., M. Ohrnberger, F. Scherbaum, M. Wathelet, and C. Cornou, 2007, Assessing the reliability of the modified three-component spatial autocorrelation technique: *Geophysical Journal International*, **168**, 779–796, doi: [10.1111/gji.2007.168.issue-2](https://doi.org/10.1111/gji.2007.168.issue-2).
- Kuiper, R. M., H. Hooijink, and M. J. Silvapulle, 2011, An Akaike-type information criterion for model selection under inequality constraints: *Biometrika*, **98**, 2, 495–501, doi: [10.1093/biomet/asr002](https://doi.org/10.1093/biomet/asr002).
- Kullback, S., and R. Leibler, 1951, On information and sufficiency: *Annals of Mathematical Statistics*, **22**, 79–86.
- Kvaerna, T., and F. Ringdahl, 1986, Stability of various  $f-k$  estimation techniques, Semiannual technical summary: NORSAR Scientific Report, 29–40.
- Lachet, C., and P. Y. Bard, 1994, Numerical and theoretical investigations on the possibilities and limitation of the Nakamura technique: *Journal of Physics of the Earth*, **42**, 377–397, doi: [10.4294/jpe1952.42.377](https://doi.org/10.4294/jpe1952.42.377).
- Lacoss, R. T., E. J. Kelly, and M. N. Toksöz, 1969, Estimation of seismic noise structure using arrays: *Geophysics*, **34**, 21–38, doi: [10.1190/1.1439995](https://doi.org/10.1190/1.1439995).
- Lenti, L., S. Martino, A. Paciello, and G. Scarascia Mugnozza, 2009, Evidence of two-dimensional amplification effects in an alluvial valley (Valnerina, Italy) from velocimetric records and numerical models: *Bulletin of the Seismological Society of America*, **99**, 1612–1635, doi: [10.1785/0120080219](https://doi.org/10.1785/0120080219).
- Lermo, J., and F. J. Chavez-Garcia, 1993, Site evaluation using spectral ratios with only one station: *Bulletin of the Seismological Society of America*, **83**, 1574–1594.
- Liu, H. P., D. M. Boore, W. B. Joyner, D. H. Oppenheimer, R. E. Warrick, W. Zhang, J. C. Hamilton, and L. T. Brown, 2000, Comparison of phase velocities from array measurements of Rayleigh waves associated with microtremor and results calculated from borehole shear-wave velocity profiles: *Bulletin of the Seismological Society of America*, **90**, 666–678, doi: [10.1785/0119980186](https://doi.org/10.1785/0119980186).
- Malischewsky, P. G., and F. Scherbaum, 2004, Love’s formula and H/V ratio (ellipticity) of Rayleigh waves: *Wave Motion*, **40**, 57–67, doi: [10.1016/j.wavemoti.2003.12.015](https://doi.org/10.1016/j.wavemoti.2003.12.015).
- Moss, R. E. S., 2008, Quantifying measurement uncertainty of thirty-meter shear-wave velocity: *Bulletin of the Seismological Society of America*, **98**, 1399–1411, doi: [10.1785/0120070101](https://doi.org/10.1785/0120070101).
- Mutua, F. M., 1994, The use of the Akaike information criterion in the identification of an optimum flood frequency model: *Hydrological Sciences Journal*, **39**, no. 3, 235–244, doi: [10.1080/02626669409492740](https://doi.org/10.1080/02626669409492740).
- Nakamura, Y., 1989, A method for dynamic characteristics estimation of subsurface using microtremor on the ground surface: Quarterly Report of the Railway Technical Research Institute of Japan, **30**, no. 1, 25–33.
- Nogoshi, M., and T. Igarashi, 1971, On the amplitude characteristic of microtremor (Part 2) (in Japanese with English abstract): *Journal of the Seismological Society of Japan*, **24**, 26–40.
- Ohori, M., A. Nobata, and K. Wakamatsu, 2002, A comparison of ESAC and  $f-k$  methods of estimating phase velocity using arbitrarily shaped microtremor analysis: *Bulletin of the Seismological Society of America*, **92**, 2323–2332, doi: [10.1785/0119980109](https://doi.org/10.1785/0119980109).
- Okada, H., and T. Matsushima, 1989, An exploration method using microtremors (1) — A theory to identify Love waves in microtremors: Proceedings of the 81st SEGJ Conference, 15–18 (in Japanese with English abstract).
- Park, C. B., R. D. Miller, and J. Xia, 1999, Multi-channel analysis of surface waves (MASW): *Geophysics*, **64**, 800–808, doi: [10.1190/1.1444590](https://doi.org/10.1190/1.1444590).
- Parolai, S., P. Bormann, and C. Milkereit, 2002, New relationships between  $V_S$ , thickness of sediments, and resonance frequency calculated by the H/V ratio of seismic noise for the Cologne area (Germany): *Bulletin of the Seismological Society of America*, **92**, 2521–2527, doi: [10.1785/0120010248](https://doi.org/10.1785/0120010248).
- Parolai, S., M. Picozzi, S. M. Richwalski, and C. Milkereit, 2005, Joint inversion of phase velocity dispersion and H/V ratio curves from seismic noise recordings using a genetic algorithm, considering higher modes: *Geophysical Research Letters*, **32**, L01303, doi: [10.1029/2004GL021115](https://doi.org/10.1029/2004GL021115).
- Picozzi, M., F. Sabetta, N. Theodoulidis, S. Zacharopoulos, A. Savvaidis, P. Y. Bard, C. Cornou, P. Gueguen, D. Fäh, I. Kalogeras, S. Akkar, D. Rinaldis, and G. Tanircan, 2007, Selected sites and available information, NERIES Project JRA4 Task C, EU-FP6 EC, Project number 026130, deliverable D1, <http://www.neries-eu.org/?subpage=/projectweb/portalproject/Deliverables.html>, accessed 28 December 2011.
- Pileggi, D., D. Rossi, E. Lunedi, and D. Albarello, 2011, Seismic characterization of rigid sites in the ITACA database by ambient vibration monitoring and geological surveys: *Bulletin of Earthquake Engineering*, **9**, 1839–1854, doi: [10.1007/s10518-011-9292-0](https://doi.org/10.1007/s10518-011-9292-0).
- Raptakis, D., F. J. Chavez-Garcia, K. Makra, and K. Ptilakis, 2000, Site effects at Euroseistest — I. Determination of the valley structure and confrontation of observations with analysis: *Soil Dynamics and Earthquake Engineering*, **19**, 1–22, doi: [10.1016/S0267-7261\(99\)00025-1](https://doi.org/10.1016/S0267-7261(99)00025-1).
- Renalier, F., and B. Endrun, 2009, Comparative analysis of classical measurements and newly developed methods, NERIES project JRA4 Task C, EU-FP6 EC project number 026130, deliverable D6, available via <http://www.neries-eu.org/?subpage=/projectweb/portalproject/Deliverables.html>, accessed 28 December 2011.
- Renalier, F., D. Jongmans, A. Savvaidis, M. Wathelet, B. Endrun, and C. Cornou, 2010, Influence of parameterization on inversion of surface wave dispersion curves and definition of an inversion strategy for sites with a strong  $V_S$  contrast: *Geophysics*, **75**, no. 6, B197–B209, doi: [10.1190/1.3506556](https://doi.org/10.1190/1.3506556).
- Richwalski, S. M., M. Picozzi, S. Parolai, C. Milkereit, F. Baliva, D. Albarello, K. Roy-Chowdhury, H. van der Meer, and J. Zschau, 2007, Rayleigh wave dispersion curves from seismological and engineering-geotechnical methods: A comparison at the Bornheim test site (Germany): *Journal of Geophysics and Engineering*, **4**, 349–361, doi: [10.1088/1742-2132/4/4/001](https://doi.org/10.1088/1742-2132/4/4/001).
- Roten, D., D. Fäh, C. Cornou, and D. Giardini, 2006, Two-dimensional resonances in Alpine valleys identified from ambient vibration wavefields: *Geophysical Journal International*, **165**, 889–905, doi: [10.1111/gji.2006.165.issue-3](https://doi.org/10.1111/gji.2006.165.issue-3).
- Sambridge, M., 1999, Geophysical inversion with a neighbourhood algorithm: I. Searching a parameter space: *Geophysical Journal International*, **138**, 479–494, doi: [10.1046/j.1365-246X.1999.00876.x](https://doi.org/10.1046/j.1365-246X.1999.00876.x).
- Sandikkaya, M. A., M. T. Yilmaz, S. B. Bakir, and Ö. Yilmaz, 2010, Site classification of Turkish national strong-motion stations: *Journal of Seismology*, **14**, 543–563, doi: [10.1007/s10950-009-9182-y](https://doi.org/10.1007/s10950-009-9182-y).

- Sandron, D., L. Sirovich, and F. Pettenati, 2011, Near-field response of a 1D-structure alluvial site: *Bulletin of the Seismological Society of America*, **101**, 2981–2997, doi: [10.1785/0120100313](https://doi.org/10.1785/0120100313).
- Savvaïdis, A., et al., 2009, Variability analysis of shallow shear wave velocity profiles obtained from dispersion curve inversion considering multiple model parametrizations: SSA Meeting 2009, Abstract in *Seismological Research Letters*, **80**, no. 2, page 354.
- Scherbaum, F., K. G. Hinzen, and M. Ohrnberger, 2003, Determination of shallow shear wave velocity profiles in the Cologne/Germany area using ambient vibrations: *Geophysical Journal International*, **152**, 597–612, doi: [10.1046/j.1365-246X.2003.01856.x](https://doi.org/10.1046/j.1365-246X.2003.01856.x).
- Semblat, J. F., M. Kham, E. Parara, P. Y. Bard, K. Pitilakis, K. Makra, and D. Raptakis, 2005, Seismic wave amplification. Basin geometry vs soil layering: *Soil Dynamics and Earthquake Engineering*, **25**, 7–10, 529–538, doi: [10.1016/j.soildyn.2004.11.003](https://doi.org/10.1016/j.soildyn.2004.11.003).
- Socco, L. V., S. Foti, and D. Boiero, 2010, Surface-wave analysis for building near-surface velocity models — Established approaches and new perspectives: *Geophysics*, **75**, no. 5, 75A83–75A102, doi: [10.1190/1.3479491](https://doi.org/10.1190/1.3479491).
- Stephenson, W. J., J. N. Louie, S. Pullammanappallil, R. A. Williams, and J. K. Odum, 2005, Blind shear-wave velocity comparison of ReMi and MASW results with boreholes to 200 m in Santa Clara Valley: Implications for earthquake ground-motion assessment: *Bulletin of the Seismological Society of America*, **95**, 2506–2516, doi: [10.1785/0120040240](https://doi.org/10.1785/0120040240).
- Sugiura, N., 1978, Further analysis of data by Akaike's information criterion and the finite corrections: *Communications in Statistics — Theory and Methods*, **A7**, no. 1, 13–26, doi: [10.1080/03610927808827599](https://doi.org/10.1080/03610927808827599).
- Tada, T., I. Cho, and Y. Shinozaki, 2009, New circular-array microtremor techniques to infer love-wave phase velocities: *Bulletin of the Seismological Society of America*, **99**, 2912–2926, October 2009, doi: [10.1785/0120090014](https://doi.org/10.1785/0120090014).
- Tokimatsu, K., 1997, Geotechnical site characterization using surface waves: 1st International Conference on Earthquake and Geotechnical Engineering, **3**, 1333–1368.
- Tuan, T. T., F. Scherbaum, and P. G. Malischewsky, 2011, On the relationship of peaks and troughs of the ellipticity (H/V) of Rayleigh waves and the transmission response of single layer over half-space models: *Geophysical Journal International*, **184**, 793–800, doi: [10.1111/gji.2011.184.issue-2](https://doi.org/10.1111/gji.2011.184.issue-2).
- van Erven, T., P. D. Grünwald, and S. de Rooij, 2008, Catching up faster by switching sooner: A prequential solution to the AIC-BIC dilemma: Cornell University, <http://arxiv.org/abs/0807.1005v1>.
- Wathelet, M., 2008, An improved neighbourhood algorithm: Parameter conditions and dynamic scaling: *Geophysical Research Letters*, **35**, L09301, doi: [10.1029/2008GL033256](https://doi.org/10.1029/2008GL033256).
- Wathelet, M., D. Jongmans, and M. Ohrnberger, 2005, Direct inversion of spatial autocorrelation curves with the neighbourhood algorithm: *Bulletin of the Seismological Society of America*, **95**, 1787–1800, doi: [10.1785/0120040220](https://doi.org/10.1785/0120040220).
- Wathelet, M., D. Jongmans, M. Ohrnberger, and S. Bonnefoy-Claudet, 2008, Array performance for ambient vibrations on a shallow structure and consequences over vs inversion: *Journal of Seismology*, **12**, 1–19, doi: [10.1007/s10950-007-9067-x](https://doi.org/10.1007/s10950-007-9067-x).
- Xia, J., R. D. Miller, and C. B. Park, 1999, Estimation of near-surface shear-wave velocity by inversion of Rayleigh waves: *Geophysics*, **64**, 691–700, doi: [10.1190/1.1444578](https://doi.org/10.1190/1.1444578).
- Xia, J., R. D. Miller, C. B. Park, J. A. Hunter, J. B. Harris, and J. Ivanov, 2002, Comparing shear waves velocity profiles inverted from multichannel surface wave with borehole measurements: *Soil Dynamics and Earthquake Engineering*, **22**, 181–190, doi: [10.1016/S0267-7261\(02\)00008-8](https://doi.org/10.1016/S0267-7261(02)00008-8).
- Xia, J., R. D. Miller, C. B. Park, and G. Tian, 2003, Inversion of high frequency surface waves with fundamental and higher modes: *Journal of Applied Geophysics*, **52**, no. 1, 45–57, doi: [10.1016/S0926-9851\(02\)00239-2](https://doi.org/10.1016/S0926-9851(02)00239-2).
- Zhao, Z., Y. Zhang, and H. Liao, 2008, Design of ensemble neural network using the Akaike information criterion: *Engineering Applications of Artificial Intelligence*, **21**, 1182–1188, doi: [10.1016/j.engappai.2008.02.007](https://doi.org/10.1016/j.engappai.2008.02.007).